This dissertation has been
microfilmed exactly as received 66-14,214

HOOD, James Dennis, 1940-
A METHOD FOR THE DETERMINATION OF
THE RADIATIVE PROPERTIES OF FLAMES.

The University of Oklahoma, Ph.D., 1966
Engineering, mechanical

University Microfilms, Inc., Ann Arbor, Michigan

Downloaded from SHAREOK. Persistent Handle URL: https://hdl.handle.net/11244/2080

THE UNIVERSITY OF OKLAHOMA

GRADUATE COLLEGE

A METHOD FOR THE DETERMINATION OF THE RADIATIVE PROPERTIES OF FLAMES

A DISSERTATION

SUBMITTED TO THE GRADUATE FACULTY

in partial fulfillment of the requirements for the

degree of

DOCTOR OF PHILOSOPHY

BY

JAMES DENNIS HOOD

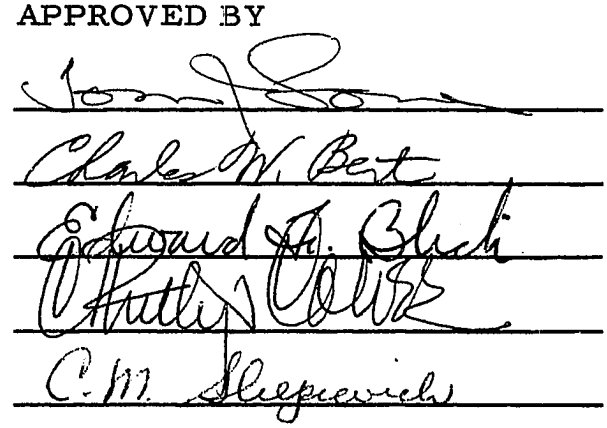
Norman, Oklahoma

1966

A METHOD FOR THE DETERMINATION OF THE

RADIATIVE PROPERTIES OF FLAMES

APPROVED BY



DISSERTATION COMMITTEE

ACKNOWLEDGEMENTS

The author wishes to express his appreciation to the many people who have contributed to the accomplishment of this study. In particular, he would like to thank Dr. T. J. Love, Jr. for his guidance throughout the Ph. D. program.

The author also wishes to thank Dr. C. M. Sliepcevich, Dr. C. W. Bert, Dr. E. F. Blick, and Dr. C. P. Colver for assisting in the preparation of this dissertation. The fellow students who have contributed to this study are too numerous to recognize individually. However, the author is appreciative of all that they have done.

A special thanks goes to my wife, Louise, who has been patiently waiting and working for the day when this dissertation would be completed.

ABSTRACT

The purpose of this study was to develop a method of predicting the total flux at a given surface from a flame of a specified size and geometry. The approach taken was to determine experimentally the monochromatic volume emission, J_λ, and the monochromatic volume absorption coefficient, β_λ, for several fuels. The transport equation for an absorbing and emitting medium was solved under the assumptions that average values for J_λ and β_λ could be used. From these equations and the experimentally determined values of J_λ and β_λ, the heat flux to surfaces from flames of larger sizes was computed. These calculations were compared with radiometer readings and shown to be in good agreement. Graphs of J_λ and β_λ for acetone, methanol, cyclohexane, n-hexane, and benzene are presented.

The frequently made assumption that a flame may be considered a system in thermodynamic equilibrium was not required in this analysis. Since the intensity scale of the monochromator had been calibrated for this experiment, it was possible to investigate the validity of the equilibrium approximation. An inductive argument was used in which the flame was considered to be an equilibrium system. Thus, using Kirchhoff's Law,

the black body intensity and the black body temperature could be computed. The temperature thus computed was found to be a strong function of wavelength indicating that the assumption of thermodynamic equilibrium was not valid for the flames tested.

TABLE OF CONTENTS

		Page
LIST OF TABLES		vii
LIST OF FIGURES		viii
Chapter		
I.	INTRODUCTION	1
II.	EQUIPMENT	9
	Spectroscope	9
	External Optics	29
	Flame Holder and Boiler	34
III.	CALIBRATIONS	37
IV.	ANALYSIS OF DATA	47
V.	DISCUSSION OF RESULTS	73
VI.	CONCLUSIONS	82
REFERENCES		87

LIST OF TABLES

Table		Page
1.	Wavelength Interval Information	30
2.	Wavelength Drum Calibration Points	38
3.	Error Analysis for Slit Width	46

LIST OF FIGURES

Figure		Page
1.	Spectrometer External Optics	7
2.	Spectrometer Internal Optics	11
3.	Optics of a Simple Spectrometer.	13
4.	Aperture Effect of the Prism	13
5.	Coordinate System for Fraunhofer Diffraction	15
6.	Graph of $I_o \frac{\sin^2\alpha}{\alpha}$	15
7.	Square Topped Intensity Pattern	15
8.	Distribution of Intensity on the Exit Slit	21
9.	Rayleigh Criterion for Resolving Power	21
10.	Geometry of Intensity Incident on the Prism.	26
11.	Diagram of Flame Holder and Boiler	36
12.	Wavelength Drum Settings vs. Wavelength.	40
13.	Acetone Flame Volume Emission (Y = 0)	48
14.	Acetone Flame Volume Absorption Coefficient (Y = 0).	49
15.	Acetone Flame Volume Emission (Y = 1/8).	50
16.	Acetone Flame Volume Absorption Coefficient (Y = 1/8). . . .	51
17.	Acetone Flame Volume Emission (Y = 1/4).	52
18.	Acetone Flame Volume Absorption Coefficient (Y = 1/4). . . .	52

Figure		Page
19.	Methanol Flame Volume Emission (Y = 0)	53
20.	Methanol Flame Volume Absorption Coefficient (Y = 0)	54
21.	Methanol Flame Volume Emission (Y = 1/8).	55
22.	Methanol Flame Volume Absorption Coefficient (Y = 1/8).	56
23.	Methanol Flame Volume Emission (Y = 1/4)	57
24.	Methanol Flame Volume Absorption Coefficient (Y = 1/4)	58
25.	Coordinate System for Flames.	59
26.	Acetone Flame Extrapolation	61
27.	Methanol Flame Extrapolation	62
28.	Cyclohexane Flame Volume Emission (Y = 0)	63
29.	Cyclohexane Flame Volume Absorption Coefficient (Y = 0)	64
30.	Cyclohexane Flame Volume Emission (z = 0)	65
31.	Cyclohexane Flame Volume Absorption Coefficient (z = 0)	66
32.	n-Hexane Flame Volume Emission (Y = 0).	67
33.	n-Hexane Flame Volume Absorption (Y = 0) Coefficient .	68
34.	n-Hexane Flame Volume Emission (z = 0).	69
35.	n-Hexane Flame Volume Absorption Coefficient (z = 0). .	70
36.	Benzene Flame Volume Emission and Absorption Coefficient (Y = 0, z = 3/4)	72
37.	Geometry for Cylindrical Flame.	75
38.	Radiation Flux versus Distance from a Cylindrical Flame	79

Figure Page

39. Black Body Temperature for an Acetone Flame. 81

40. Radiation Flux versus Distance from a Cylindrical Acetone Flame 83

41. Radiation Flux versus Distance from a Cylindrical Methanol Flame 84

42. Comparison of Absorption and Emission 85

A METHOD FOR THE DETERMINATION OF THE RADIATIVE PROPERTIES OF FLAMES

CHAPTER I

INTRODUCTION

The object of this research was to develop a method of predicting the radiative heat flux from a flame of an arbitrary size and geometry. The analysis of the flame was based on the transport equation for an absorbing and emitting medium. Measurements of the monochromatic volume absorption coefficient and the monochromatic volume emission were made on a small laboratory-size flame. These parameters were then used in a computer program to predict the radiative flux from larger flames.

The principal difference between this approach and previous work (1, 2) on the prediction of radiative heat flux from flames was the use of the transport equation to determine the emitted radiation. The general approach taken by the previous workers was to determine the radiated intensity from the temperature and emittance of the flame. These two parameters were measured by somewhat different means but

they all assumed that a flame may be considered a system in thermodynamic equilibrium.

Temperature measurements in flames have been discussed by Broida (3). He concluded that "There have been a large number of 'temperature' determinations in hot gases and flames above 1500° K. While these measurements have been of value for comparison purposes, it is strikingly clear from the literature that methods have not yet been developed which give practical measurements of temperature. Probably this is caused more by temperature gradients and nonequilibrium in the hot gases than by the methods of 'temperature' measurement."

The determination of the emittance of the flame in references (1, 2) was made by measuring the absorptance of a flame and equating it to the emittance by Kirchhoff's Law. Kirchhoff's Law can be derived only for a system which is in thermodynamic equilibrium with its surroundings. Since a flame does not represent a system in thermodynamic equilibrium, the applicability of Kirchhoff's Law must be questioned. In Chapter V the applicability of Kirchhoff's Law to flames will be discussed in more detail.

The analysis of the phenomena of combustion and a complete description of the chemical reactions occurring in a flame would be in itself a formidable task. However, spectrograms of the infrared radiation emitted by a flame indicated that such a rigorous analysis was not necessary. The majority of the radiation emitted by the flame appeared

as a continuum which is probably emitted by the hot carbon particles. The vibrational energy band of the CO_2 molecules which appeared in the 4.2 to 4.6 micron wavelength interval also gave a significant contribution to the total emitted energy. For acetone and methanol the CO_2 radiation gave a very significant contribution to the total intensity. However for benzene, the continuum is sufficiently intense that the contribution of the CO_2 radiation was fairly small. An intensity peak at the 3.3 to 3.5 micron wavelength interval due to the C-H vibrational energy bands was usually present near the base of the flame. A flame which is chemically reacting and is radiating a large percent of its energy does not represent an equilibrium system. In the reaction zone there is certainly not an equilibrium situation and even in the outer cone the carbon particles and the CO_2 molecules do not appear to have time to equilibrate their energy. Large flames may indeed approach an equilibrium distribution of energy and for small flames of materials such as benzene an equilibrium may be approached. However, in general, the thermodynamic equilibrium assumption must be questioned for flames.

For these reasons an analysis for the radiation from a flame was proposed for this experiment which does not require an equilibrium assumption but rather was based on the differential equation describing the intensity of radiation as a function of optical path length in a flame.

The transport equation for the intensity in an absorbing and emitting medium is:

$$\frac{dI_\lambda}{dx} = -\beta_\lambda(x)I_\lambda + J_\lambda(x) \tag{1}$$

where

I_λ is the monochromatic intensity

x is the optical path length

β_λ is the monochromatic volume absorption coefficient

J_λ is the monochromatic volume emission

introducing an integrating factor

$$\frac{dI_\lambda}{dx}\, e^{\int \beta_\lambda(x)\,dx} + \beta_\lambda(x) I_\lambda\, e^{\int \beta_\lambda(x)\,dx} = J_\lambda(x)\, e^{\int \beta_\lambda(x)\,dx} \tag{2}$$

or

$$\frac{d}{dx}\left(I_\lambda\, e^{\beta_\lambda(x)\,dx}\right) = J_\lambda(x)\, e^{\int \beta_\lambda(x)\,dx} \tag{3}$$

It is not possible, however, to determine experimentally the functional relationship between β_λ and x. The value for β_λ determined by this experiment was the average of $\beta_\lambda(x)$ over the optical path length of the flame observed. There is, of course, some question of whether the same average value of β_λ will apply to the larger flames. Experimental evidence, which will be discussed later, indicates that such an assumption holds for practical purposes

$$I_\lambda\, e^{\beta_\lambda x} = \int J_\lambda(x)\, e^{\beta_\lambda x}\,dx + c \tag{4}$$

Again the same argument of experimentally determining an average J_λ

was used to obtain:

$$I_\lambda e^{\bar{\beta}_\lambda x} = \frac{\bar{J}_\lambda e^{\bar{\beta}_\lambda x}}{\bar{\beta}_\lambda} + c \tag{5}$$

or

$$I_\lambda = \frac{\bar{J}_\lambda}{\bar{\beta}_\lambda} + c\, e^{-\bar{\beta}_\lambda x} \tag{6}$$

From the boundary condition $I_\lambda = 0$ at $x = 0$, a value for c may be obtained and the equation becomes:

$$I_\lambda = \frac{\bar{J}_\lambda}{\bar{\beta}_\lambda} (1 - e^{-\bar{\beta}_\lambda x}) \tag{7}$$

For a flame having an optical path length of a, the intensity emitted is given by:

$$I_{\lambda b} = \frac{\bar{J}_\lambda}{\bar{\beta}_\lambda} (1 - e^{-\bar{\beta}_\lambda a}) \tag{8}$$

However, if the flame is illuminated by a source of intensity $I_{\lambda c}$ the evaluation of the constant in equation (6) gives

$$I_\lambda = \frac{\bar{J}_\lambda}{\bar{\beta}_\lambda} (1 - e^{-\bar{\beta}_\lambda x}) + I_{\lambda c}\, e^{-\bar{\beta}_\lambda x} \tag{9}$$

which for a flame of optical path length a becomes:

$$I_{\lambda a} = I_{\lambda b} + I_{\lambda c}\, e^{-\bar{\beta}_\lambda a} \tag{10}$$

Thus $\bar{\beta}_\lambda$ may be determined from equation (10) and knowing this, $\bar{J}_\lambda$ may be computed from equation (8) since the spectrometer was calibrated in terms of intensity. Putting these values back into equation

(7), one may determine the emitted intensity from a flame of any optical path length.

Figure 1 is a schematic layout of the optical system used to make the intensity measurements. Mirror M_2 focused the radiation from the flame onto the entrance slit of a Perkin-Elmer Model 12-C Spectrometer. Mirror M_3 focused the image of the globar in the same plane as the object plane of mirror M_2. Mirrors M_1 and M_4 are plane mirrors.

The procedure for obtaining the measured values of $I_{\lambda a}$, $I_{\lambda b}$ and $I_{\lambda c}$ was as follows. First, a spectrogram was taken of the sum of the intensity emitted by the flame and that portion of the intensity emitted by the globar which was transmitted through the flame. A shutter was then placed in front of the globar and a spectrogram of the intensity emitted by the flame was taken. The temperature of the globar was recorded throughout the first spectrogram. Since the output of the spectrometer had been calibrated in terms of intensity, $I_{\lambda a}$ could be determined from the first spectrogram and $I_{\lambda b}$ could be determined from the second spectrogram. The temperature of the globar was found to vary somewhat due to line voltage fluctuations. Thus, in order to determine the intensity incident on the flame $I_{\lambda c}$ from the temperature of the globar, a reference intensity calibration curve was taken just prior to igniting the flame. The reference intensity calibration, $I_{\lambda r}$, was a scan of the intensity of just the globar taken simultaneously with a temperature record of the globar, T_r. Then, knowing the temperature of the globar,

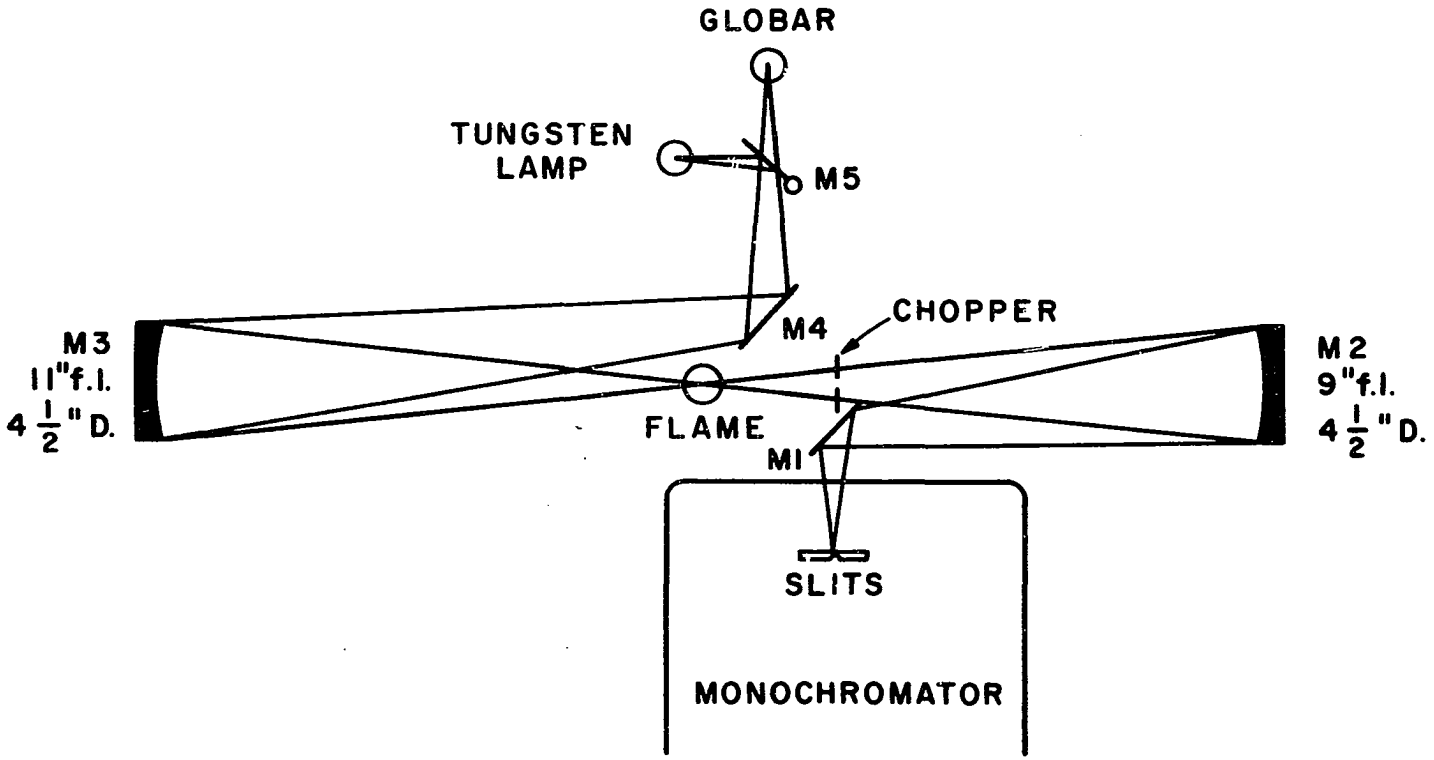


Figure 1. Spectrometer External Optics

T_c, during the data runs to determine the absorption coefficient of the flame, the intensity $I_{\lambda c}$ could be determined from

$$I_{\lambda c} = \frac{I_{\lambda r}(e^{c_2/\lambda T_r} - 1)}{(e^{c_2/\lambda T_c} - 1)}$$

The wavelength calibrations of the spectrometer were made by observing several absorption peaks of 1, 2, 4 trichlorobenzene, toluene, polystyrene, and didymium glass. The wavelength of several absorption peaks have been accurately determined by Plyler(4, 5, 6). The wavelength calibrations of the Model-12C Perkin-Elmer Spectrometer then became a matter of identifying the absorption peaks identified by Plyler and measuring their locations with respect to the setting of the wavelength drum on the spectrometer.

Absolute intensity calibrations of a spectrometer involved finding the relationship between the output of the radiation detector and intensity incident on its front slit. To determine this relationship several effects of the external and internal optics had to be described properly. All of the effects described will be discussed in more detail in Chapters II and III.

CHAPTER II

EQUIPMENT

Spectrometer

The spectrometer used in this experiment was a Perkin-Elmer Model 12-C Single Pass Infrared Spectrometer. Complete sets of NaCl and quartz optics were available which in conjunction with the thermocouple, lead sulfide, and photomultiplier detectors gave a capability of observing the spectrum from 0.5 to 15 microns. The spectrometer was used to obtain the intensity versus wavelength data from which $\overline{\beta}_\lambda$ and $\overline{J}_\lambda$ were computed. In order to interpret these data properly, several parameters of the spectrometer and the external optics had to be analyzed.

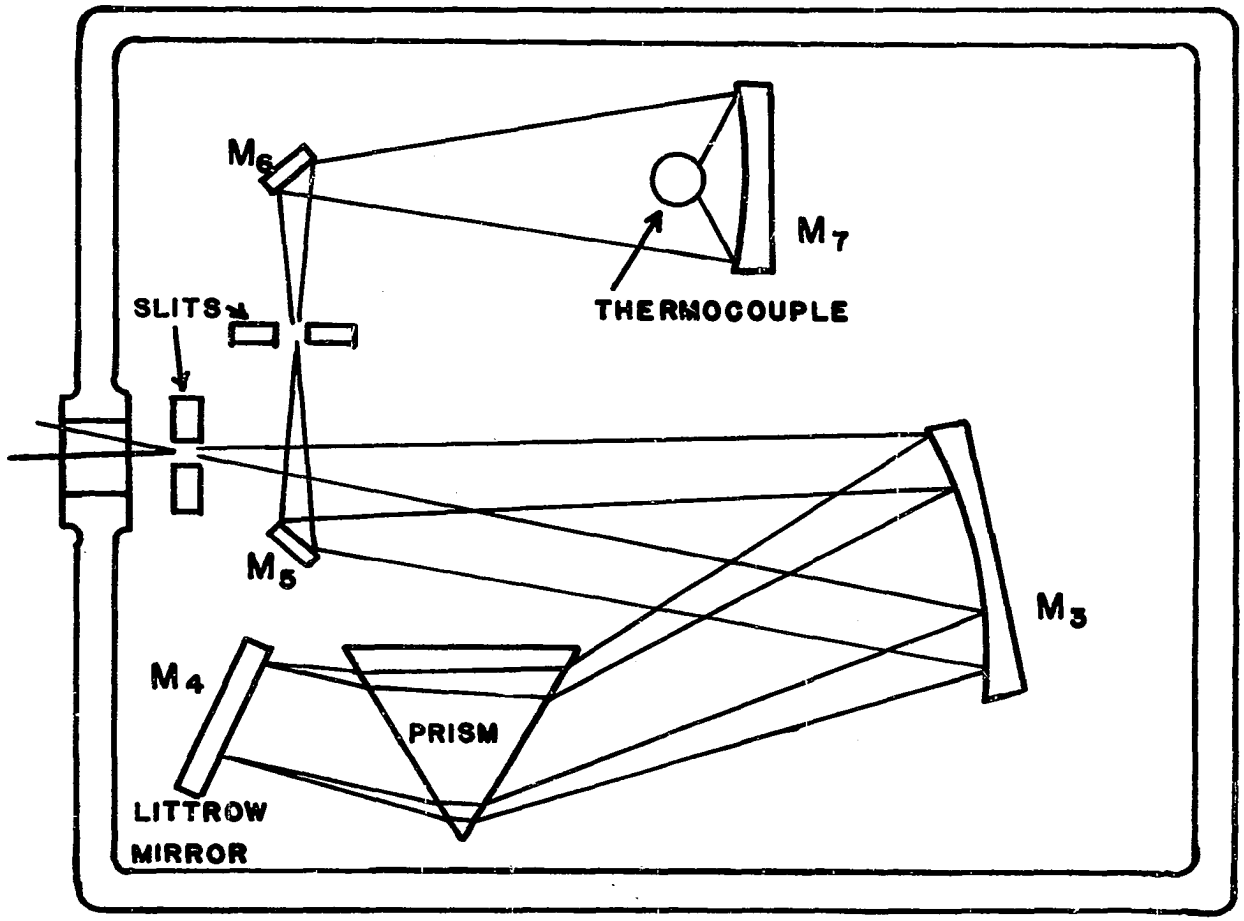
The external optics system used in this experiment is shown in Figure 1. This system focuses the image of the radiation source onto the plane of the front slit of the spectrometer. Thus, the front slit determines the area of the source which the spectrometer observes. The back slit determined what wavelength increment of the spectra was observed by the detector. The effect of these slits was analyzed in order to determine a good compromise for the setting of the slit width. The slits must be set wide enough apart to insure good spectral purity;

however, the spectral half width increases as the slit width increases and it is desirable to have a small spectral half width.

The effects of the slits for a system where the radiation source was focused onto the plane of the entrance slit was analyzed on the basis of the following arguments. The source was considered to be divided into infinitesimal regions and the radiation was divided into infinitesimal wavelength intervals. Thus, the effect of a monochromatic point source was considered. Once the effect of a monochromatic point source was understood, the effect of a finite size continuum source could be argued.

The source of radiation for this experiment was either a globar or the flame. Therefore, the radiation passing through the entrance slit was essentially noncoherent since each point on the source emitted radiation which had no fixed phase relation with the radiation emitted from any other point on the source. It was important to make the distinction between coherent and noncoherent radiation because there would be no diffraction pattern caused by the entrance slit for noncoherent radiation. No source is completely coherent or noncoherent but for a finite size source with an image formed on the entrance slit the noncoherent approximation is quite good (7). Thus, it was assumed that the diffraction effect of the entrance slit could be neglected.

The effect of a point source placed at the entrance slit of the spectrometer was considered. Figure 2 is a layout of the internal optics of the Model 12-C Perkin-Elmer Spectrometer. In this instrument



PERKIN-ELMER MODEL 12-C SPECTROMETER

Figure 2. Spectrometer Internal Optics

mirror M3 is the collimator and the telescope mirror. This has the same effect as the collimator lens and the telescope lens in the optic system of the simple spectroscope shown in Figure 3. The two systems are equivalent as far as the slit effects are concerned. Thus, the simple spectroscope in Figure 3 was analyzed, since it is easier to visualize the diffraction phenomena on this spectroscope.

The effect of the prism is twofold. First, it disperses the radiation into its spectrum and second, for the Model 12-C spectrometer, it is the limiting aperture for the light path through the spectrometer. Considering only a monochromatic light source, the discussion may be further simplified since the bending of the rays by the prism may be neglected and only the limiting aperture effect of the prism will be considered. Figure 4 shows the optic system considering only the aperture effect of the prism.

The aperture effect of the prism will give rise to a diffraction pattern in the focal plane of the telescope lens. To determine completely the shape of the diffraction pattern produced by a point source in the entrance slit, it is necessary to consider both the width and height of the aperture. This pattern is called the Fraunhofer diffraction pattern for a rectangular aperture. Rossi (8) gave a rigorous treatment of this and derived the expression

$$I_P = I_0 \left(\frac{\sin^2 \alpha}{\alpha^2} \right) \left(\frac{\sin^2 \beta}{\beta^2} \right) \qquad (11)$$

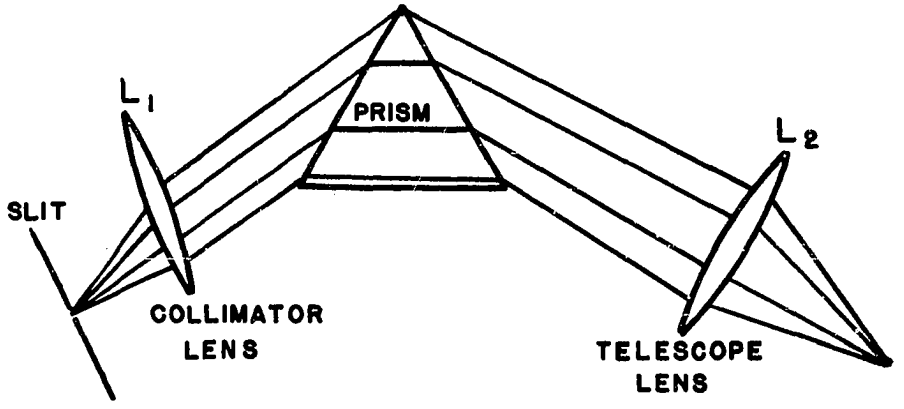


FIGURE 3. OPTICS OF A SIMPLE SPECTROMETER

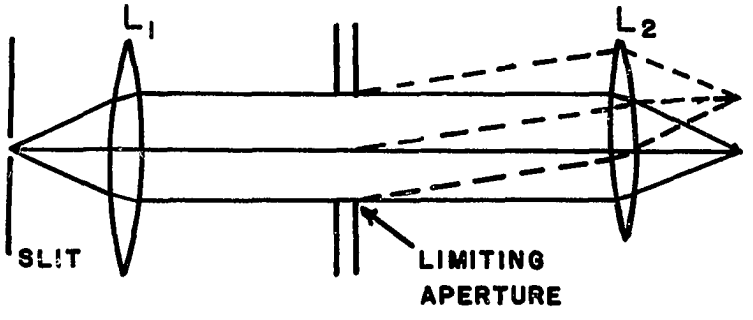


FIGURE 4. APERTURE EFFECT OF THE PRISM

for the intensity at any point P in the focal plane of the telescope lens. Figure 5 shows the coordinate system used in conjunction with this expression. The quantities α and β are given by the expressions

$$\alpha = \frac{\pi a Y}{f \lambda} \tag{12}$$

$$\beta = \frac{\pi b Z}{f \lambda} \tag{13}$$

where Y and Z are the coordinates in the focal plane of the telescope lens, Σ, a and b are the width and height of the effective aperture of the prism, f is the focal length of the telescope lens, and λ is the wavelength. Equation 11 gives the intensity as a function of the intensity at the center of the diffraction pattern in the focal plane. The intensity distribution along the Y axis ($\beta = 0$) is given by

$$I_P = I_0 \frac{\sin^2 \alpha}{\alpha^2} \tag{14}$$

which is graphed in Figure 6. The maxima and minima of equation 14 are given by

$$\sin\alpha(\alpha \cos\alpha - \sin\alpha) = 0 \tag{15}$$

The values of α which satisfy this equation are determined from

$$\sin\alpha = 0 \quad \text{and} \quad \tan\alpha = \alpha \tag{16}$$

The values of α which satisfy $\sin\alpha = 0$, $\alpha = \pm n\pi$ where n = 1, 2, 3, ---, will give the minimum values of I_P. The maxima of equation 14 are

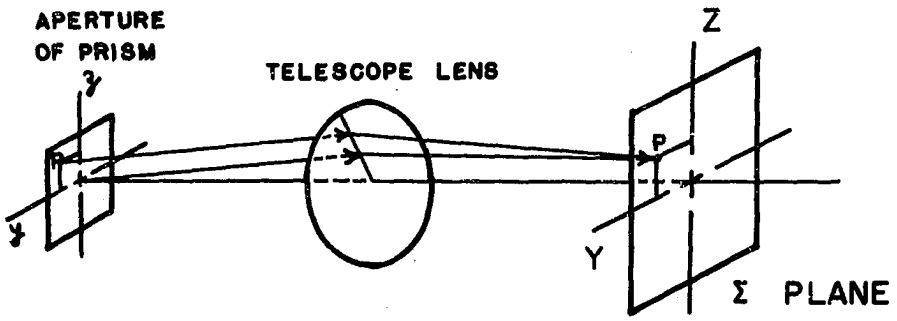


FIGURE 5. COORDINATES FOR FRAUNHOFER DIFFRACTION

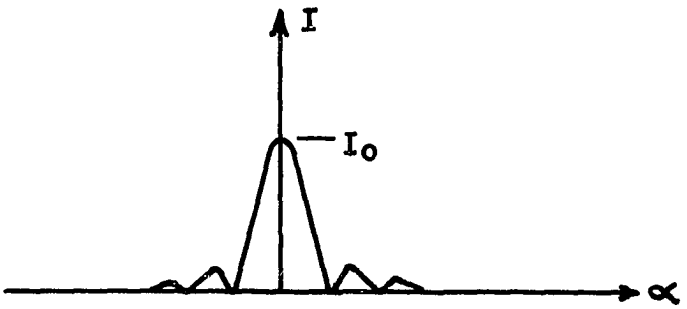


FIGURE 6. GRAPH OF $\frac{I_0 \sin^2 \alpha}{\alpha}$

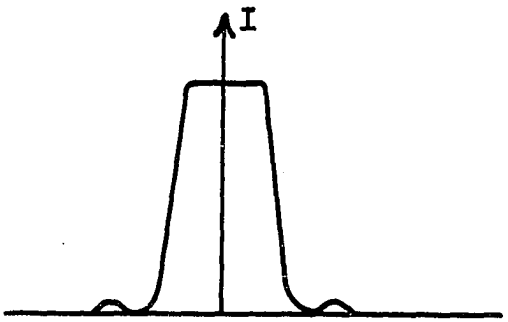


FIGURE 7. SQUARE-TOPPED INTENSITY PATTERN

for the values of α which satisfy the transcendental equation $\tan\alpha = \alpha$. The first four values of α which satisfy the transcendental equation are 0, 4.493, 7.725, and 10.904. The values of intensity for the central maximum and the next three maxima are

$$\begin{aligned} I_P &= I_0 && \text{central maximum} \\ I_P &= 0.0472\, I_0 && \text{second maximum} \\ I_P &= 0.0159\, I_0 && \text{third maximum} \\ I_P &= 0.0083\, I_0 && \text{fourth maximum} \end{aligned} \tag{17}$$

The distance ξ to the first diffraction minimum on the line $Z = 0$ in the plane Σ occurs at $\alpha = \pi$ or from equation 12

$$\alpha = \pi = \frac{\pi a Y}{f \lambda} \tag{18}$$

$$Y = \frac{f\lambda}{a} \tag{19}$$

For the Model 12-C Perkin Elmer Spectrometer, f = 27 centimeters and a is approximately 7 centimeters; so, for the wavelength of $\lambda = 5$ microns, Y = 21.7 microns.

The preceding discussion considered the diffraction pattern due to a point source. This represents in practice the effect of an entrance slit whose geometric image onto the plane Σ is very narrow as compared to the width of the central diffraction maximum. For the five-micron case calculated above the central maximum would be 45.4 microns

in width, so an entrance slit whose geometric projection on the focal plane is 2 microns wide would produce this diffraction pattern. The Model 12-C spectrometer has the same focal lengths for the collimator and the telescope giving a magnification of 1 for the optical system. Thus, the geometric projection of the entrance slit onto the Σ plane is the same size as the entrance slit.

Since the radiation source was considered to be noncoherent, there is no diffraction pattern caused by the entrance slit. Thus, the effect of opening the slit to three times its original width is the same as placing another slit like the original slit on either side of it. The intensity pattern on the Σ plane is equal to the sum of three patterns of the type shown in Figure 6 except that the central maxima of the two new patterns are displaced slightly. The effect of opening the entrance slit from a very thin slit to a slit width three times its original width is to increase the peak intensity to approximately three times its original value while increasing the width of the central maximum only slightly.

Further increasing the slit width has the effect of adding more thin slits to the side of the original slit and the intensity pattern is equal to the sum of many thin-slit diffraction patterns all slightly displaced. The addition of the diffraction patterns has the effect of increasing the intensity of the central maximum as the slit is widened. However, when the slit is wide enough that its geometric image on the Σ plane is equal

to the width of the central diffraction maximum of the thin slit, further increasing the width of the entrance slit will add negligibly to the intensity at the point Y = 0. This is true because the second, third, etc. maxima are quite small as compared to the central maximum. As the entrance slit is opened beyond this width the effect is to increase the width of the pattern on the Σ plane without increasing the intensity at the point Y = 0 thus creating a square-topped intensity pattern as shown in Figure 7. In most applications and for absolute intensity calibrations in particular, it is desirable to have a flat-topped intensity pattern on the Σ plane since under these circumstances the effect of diffraction may be neglected. Also, the image in the Σ plane may be assumed to be the optical image of the entrance slit as determined by geometric optics.

From the preceding considerations, it is necessary to use a slit width of 45.4 microns to obtain a flat-topped pattern at a wavelength of 5 microns. Thus, an entrance slit width of 100 microns was used in these experiments to insure that diffraction effects were negligible over the wavelength interval used (1 to 6 microns).

In the Model 12-C spectrometer a second slit is placed in the focal plane of the telescope. This slit is mechanically connected to the entrance slit and, thus, always has the same width. The effect of this slit is to pass only a portion of the intensity into the detector. If the diffraction effect is negligible, the intensity at the exit slit will be an

image of the intensity passed by the entrance slit. Since the source of radiation was assumed to be noncoherent, there will be no diffraction due to the exit slit.

The effect of a continuum light source rather than a monochromatic light source must be analyzed to complete the discussion of slit effects. Since the diffraction effects are negligible for a slit width of 0.1 millimeters, the intensity pattern in the plane of the exit slit is the optical projection of the entrance slit. The dispersive effect of a prism is to bend the intensity of a given wavelength through a fixed angle and, thus, determine the location of the image of the entrance slit on the exit slit plane. The angle through which the intensity beam is bent by the prism will depend on its wavelength. Thus, for every infinitesimal wavelength interval there will be an image of the entrance slit at a different place on the exit plane. For a continuum radiation source there will be overlapping of the entrance slit images from many wavelength increments on the exit slit.

The following argument can be used to construct the intensity distribution versus wavelength at the exit slit for a continuum radiation source. Since the entrance and exit slits are always the same width and since the optical system has a magnification of unity, the width of the image of the entrance slit coincides with the width of the exit slit for some wavelength λ_0. For the wavelengths $\lambda_0 \pm \delta\lambda$, where $\delta\lambda$ is some small increment of wavelength, the image of the entrance slit

will be displaced slightly with respect to the exit slit due to the dispersion of the prism. For these wavelengths part of the intensity will be blocked from passage through the exit slit. As $\delta\lambda$ increases, a larger amount of the intensity will be blocked from passage through the exit slit until finally at $\lambda = \lambda_0 \pm \Delta\lambda$ all intensity will be blocked and for all wavelengths outside this interval there will be no contribution to the intensity passing through the exit slit. The limiting wavelength increment, $\Delta\lambda$, equals the wavelength increment covered by the finite width of the exit slit. Figure 8 shows the distribution of wavelength versus the ratio of the monochromatic intensity passed through the exit slit to the monochromatic intensity incident on the plane of the exit slit. To determine the total intensity passing through the exit slit, the integral of I_λ, the incident intensity on the entrance slit, times the shape of the distribution function shown in Figure 8 must be performed. Thus, the intensity passing through the exit slit is

$$I = \int_{\lambda_0-\Delta\lambda}^{\lambda_0} I_\lambda \left[\frac{\lambda}{\Delta\lambda} - \frac{1}{\Delta\lambda}(\lambda_0 - \Delta\lambda)\right] d\lambda$$

$$+ \int_{\lambda_0}^{\lambda_0+\Delta\lambda} I_\lambda \left[-\frac{\lambda}{\Delta\lambda} + \frac{1}{\Delta\lambda}(\lambda_0 + \Delta\lambda)\right] d\lambda \qquad (20)$$

The wavelength increment, $\Delta\lambda$, versus λ will be computed later. However, for a 0.1 millimeter exit slit width $\Delta\lambda$ is quite small

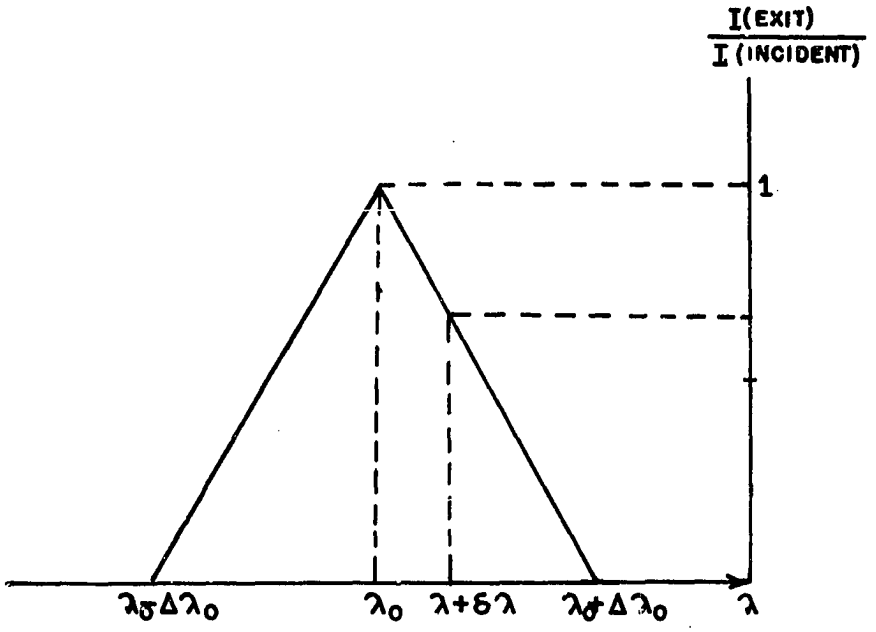


FIGURE 8. INTENSITY FUNCTION AT THE EXIT SLIT

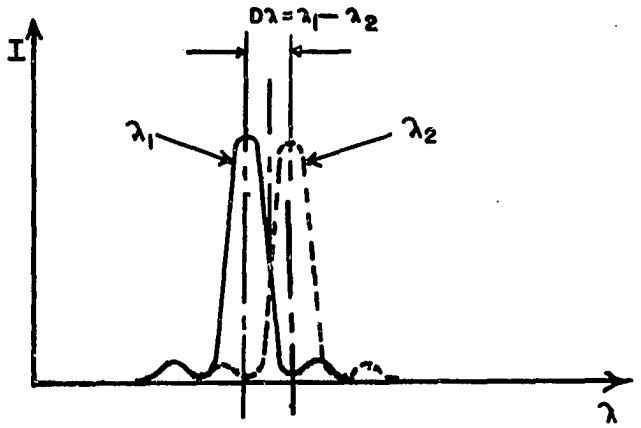


FIGURE 9. RAYLEIGH CRITERION FOR RESOLVING POWER

and the mean value rule may be used to evaluate the above equation rather than performing the actual integral. Thus, the intensity passed by the exit slit is given approximately by

$$I = \Delta\lambda I_{\lambda 0}. \tag{21}$$

An analysis of the error introduced by using the mean value rule for integration will be discussed in Chapter III.

The diffraction effects discussed above give a lower limit to the slit width for the spectroscope. The upper limit is determined from the relationship between the mechanical slit width and the spectral slit width. It was desirable to have as small a spectral slit width as possible. Thus, the limiting slit width determined from the diffraction effect of 0.1 millimeter was used.

The Model 12-C Perkin-Elmer Spectrometer is a Littrow type prism spectrometer with internal optics shown schematically in Figure 2. The Littrow mirror is placed normal to the dispersed beam emerging from the prism. For some particular wavelength, as determined by the orientation of the mirror, the emergent beam is passed back through the prism and focused by the telescope onto the exit slit. The spectrum is scanned by rotating the Littrow mirror.

The spectral slit width, $\Delta\lambda$, of the exit slit is the sum of two terms. The first term may be computed from the dispersion, $d\theta/d\lambda$, of the prism and optical system where θ is the angle through which the

beam is bent by the prism. The second term is the Rayleigh term which accounts for the resolving power of the telescope. This term is computed from consideration of how far apart two objects must be in order for a telescope to distinguish them. Due to the dispersion of the prism the image of the entrance slit is displaced for different wavelengths. Thus, the Rayleigh term determines the minimum wavelength interval which can be resolved by a spectrometer. The two terms must be added to determine the spectral slit width, since the first term computes the spectral slit width if the telescope could precisely resolve two objects and the second term determines the additional spectral interval due to the fact that the wavelength can only be determined to within a certain interval $\Delta\lambda_R$.

The equation for the spectral slit width may be derived from the following argument. The angular dispersion of the Model 12-C spectrometer, $\Delta\theta/\Delta\lambda$, may be equated to two times the angular dispersion of the prism since for a Littrow mount spectrometer the radiation passes through the prism twice.

$$\frac{\Delta\theta}{\Delta\lambda_0} \approx 2\,\frac{d\theta}{d\lambda} = \frac{d\theta}{dn}\,\frac{dn}{d\lambda} \qquad (22)$$

where n is the index of refraction of the prism material. The expression for $d\theta/dn$ may be computed from the equation for the index of refraction for a prism.

$$\frac{d\theta}{dn} = \frac{2 \sin(A/2)}{\left[1 - n^2 \sin^2(A/2)\right]^{1/2}} \tag{23}$$

where A is the apex angle of the prism.

Combining these two equations yields

$$\Delta\lambda_D = \frac{\left[1 - n^2 \sin^2(A/2)\right]^{1/2} \Delta\theta}{2 \frac{dn}{d\lambda} \left[2 \sin(A/2)\right]} \tag{24}$$

The $\Delta\theta$ of interest for computing the spectral slit width for the exit slit is given by

$$\Delta\theta = S/d \tag{25}$$

where S is the mechanical slit width and d is the focal length of the telescope. The spectral slit width due to the dispersion of the prism is given by

$$\Delta\lambda_D = \frac{\left[1 - n^2 \sin^2(A/2)\right]^{1/2}}{4 \frac{dn}{d\lambda} \sin(A/2)} \frac{S}{d} \tag{26}$$

To compute the Rayleigh term, $\Delta\lambda_R$, a source emitting two monochromatic lines will be considered. The prism will separate these two wavelengths so that two images of the entrance slit separated by some distance will be presented to the telescope. Diffraction will occur in the telescope even if the entrance slit is open wide enough to eliminate Fraunhofer diffraction. Rayleigh's criterion for determining when two lines can be resolved by a telescope is that the central maximum of one diffraction pattern must be centered over the first minimum

of the second pattern. Figure 9 gives the coordinate system for this discussion. The angle θ represents the angular separation between the central maximum and the first diffraction minimum. For the Rayleigh criterion to be fulfilled, this must be equal to the angular separation Φ of the two images. For the distance ξ to coincide with the first diffraction minimum of the diffracted image of λ_1, the expression for θ must be

$$\sin\theta = \lambda/a \tag{27}$$

where a is the limiting aperture. For small angles this may be approximated by

$$\theta = \lambda/a \tag{28}$$

This result is true only for rectangular aperture. However, since the prism acts as the limiting aperture in the Model 12-C spectrometer, this equation is valid for this analysis.

Equation 22 is valid for the Rayleigh term

$$\frac{\Delta\lambda_R}{\Delta\theta} = \frac{1}{2}\frac{dn}{d\theta}\frac{d\lambda}{dn} \tag{29}$$

The Rayleigh term accounts for the angular separation of two lines in order for them to be resolved. Therefore, the angular separation $\Delta\theta$ for equation 29 must be the minimum angular separation of two lines which can be resolved and, thus, equals λ/a as shown in equation 28. If the incident beam completely fills side AB of the prism in Figure 10

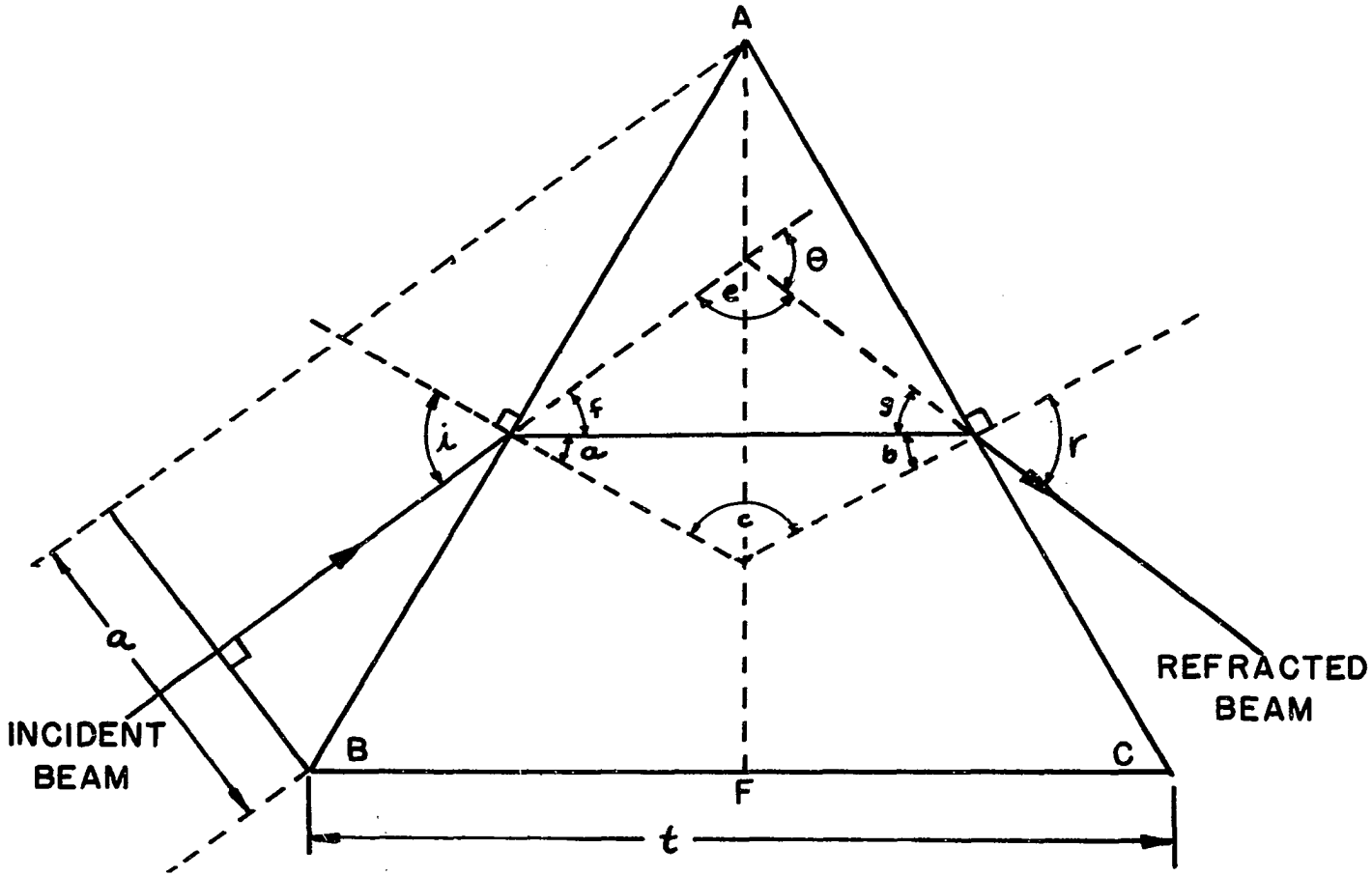


Figure 10. Geometry of Intensity Incident on the Prism

it can be shown that

$$\cos i = \frac{a}{AB} \tag{30}$$

and since

$$\sin \frac{A}{2} = \frac{BF}{AB} \tag{31}$$

then

$$t = 2AB \sin(A/2) \tag{32}$$

where t is the thickness of the base of the prism. Combining equations 30 and 32

$$\frac{t}{a} = \frac{2 \sin(A/2)}{\cos i} = \frac{2 \sin(A/2)}{(1 - \sin^2 i)^{1/2}} \tag{33}$$

or using Snell's law of refraction

$$\frac{t}{a} = \frac{2 \sin(A/2)}{(1 - n^2 \sin^2 a)^{1/2}} \tag{34}$$

For a prism adjusted for the angle of minimum deviation as shown in Figure 10, the angle a equals the angle A/2 so equation 34 becomes

$$\frac{t}{a} = \frac{2 \sin(A/2)}{\left[1 - n^2 \sin^2(A/2)\right]^{1/2}} \tag{35}$$

A comparison of equations 23 and 35 shows that

$$\frac{t}{a} = \frac{d\theta}{dn} \tag{36}$$

Substituting equation 36 and the expression $\Delta\theta = \lambda/a$ into equation 29

gives

$$\Delta\lambda_R = \frac{1}{2}\frac{d\lambda}{dn}\left(\frac{a}{t}\right)\left(\frac{\lambda}{a}\right) = \frac{\lambda}{2t\,\frac{dn}{d\lambda}} \tag{37}$$

As discussed above, the spectral slit width, $\Delta\lambda$, is given by

$$\Delta\lambda = \Delta\lambda + \Delta\lambda_R \tag{38}$$

or

$$\Delta\lambda = \frac{\left[1 - n^2 \sin^2(A/2)\right]^{1/2}}{4\,\frac{dn}{d\lambda}\sin(A/2)}\,\frac{S}{d} + \frac{\lambda}{2t\,\frac{dn}{d\lambda}} \tag{39}$$

Thus, the spectral slit width is a function of the exit slit width, S. It was desirable to use a small spectral slit width in this experiment since the detectors receive energy from a wavelength range of $2\Delta\lambda$. Thus, a compromise must be made in choosing the slit width, since the slit must be wide enough to minimize the effect of Fraunhofer diffraction but must be kept narrow to give a small spectral slit width.

Values of the index of refraction, n, as a function of wavelength were recorded by Baly (9). The empirical curve fit which he recorded for these data is given by

$$n^2 = a^2 + \frac{M_1}{\lambda^2 - \lambda_1^2} - \frac{M_2}{\lambda_2^2 - \lambda^2} \tag{40}$$

where $a^2 = 5.1790$, $M_1 = 0.018496$, $\lambda_1^2 = 0.01621$, $M_2 = 8977.0$, $\lambda_2^2 = 3149.3$ and λ is wavelength in microns. The derivative of the index of

refraction with respect to wavelength may be computed from equation 40 and used in equation 39 to determine $\Delta\lambda$. For the Model 12-C Perkin-Elmer Spectrometer with a NaCl prism the values for the quantities in equation 39 are as follows: A, the apex angle of the prism, is 60^{o}; d, the focal length of the telescope mirror, is 27 centimeters; and t, the length of the base of the prism, is 7.5 centimeters. Table 1 gives the computed values of $\Delta\lambda$, $\Delta\lambda_D$, $\Delta\lambda_R$, n, and $dn/d\lambda$ as a function of wavelength for a slit width of 0.100 millimeters.

The Model 12-C spectrometer was used to scan wavelength continuously. The Littrow mirror was rotated by a mechanical linkage and a motor driven shaft to scan the spectrum past the fixed exit slit. It was necessary for the rate of scanning to be slow enough that the change in wavelength per period of the chopper due to scanning be small as compared to the $\Delta\lambda$ being viewed by the detector. For the wavelength range, 1.5 to 5.2 microns, used in this experiment and the scanning speed of 8 minutes per revolution of the drive shaft, each cycle of the 13-cycle-per-second chopper represents a shift in the wavelength at the exit slit due to scanning of 0.0004 microns. Since the minimum λ for a slit width of 0.100 millimeter is approximately 0.028 microns in the wavelength region of interest, the effect of scanning was considered negligible.

External Optics

An optical system external to the spectrometer was required to determine the radiation parameters for the flame. This system focused

a small area of the flame onto the entrance slit of the spectrometer and focused the image of the radiation source onto the same area of the flame. It was also necessary to minimize the effect of aberrations and to design a system which would fill the collimator of the spectroscope with radiation. Figure 1 is a layout of the optical system used in this experiment.

TABLE I

WAVELENGTH INTERVAL INFORMATION

λ	$\Delta\lambda$	$\Delta\lambda_D$	$\Delta\lambda_R$	n	$dn/d\lambda$
1.0	0.00962	0.00911	0.00051	1.5318	0.01307
1.2	0.01618	0.01516	0.00102	1.5298	0.00787
1.4	0.02423	0.02248	0.00175	1.5285	0.00531
1.6	0.03302	0.03031	0.00271	1.5276	0.00394
1.8	0.04155	0.03776	0.00379	1.5269	0.00317
2.0	0.04897	0.04406	0.00491	1.5263	0.00272
2.2	0.05474	0.04876	0.00598	1.5258	0.00246
2.4	0.05874	0.05182	0.00692	1.5253	0.00231
2.6	0.06114	0.05341	0.00773	1.5248	0.00224
2.8	0.06224	0.05386	0.00838	1.5244	0.00223
3.0	0.06238	0.05346	0.00892	1.5239	0.00224
3.2	0.06184	0.05250	0.00934	1.5235	0.00229
3.4	0.06084	0.05118	0.00966	1.5230	0.00235
3.6	0.05957	0.04964	0.00993	1.5226	0.00242
3.8	0.05813	0.04800	0.01013	1.5221	0.00250
4.0	0.05661	0.04633	0.01028	1.5216	0.00259
4.2	0.00507	0.04467	0.01040	1.5210	0.00269
4.4	0.05354	0.04305	0.01049	1.5205	0.00279
4.6	0.05205	0.04148	0.01047	1.5199	0.00290
4.8	0.05061	0.03998	0.01063	1.5193	0.00301
5.0	0.04922	0.03855	0.01067	1.5187	0.00313
5.2	0.04790	0.03720	0.01070	1.5181	0.00324
5.4	0.04663	0.03591	0.01072	1.5174	0.00336
5.6	0.04543	0.03470	0.01073	1.5167	0.00348
5.8	0.04429	0.03355	0.01074	1.5160	0.00360
6.0	0.04320	0.03246	0.01074	1.5153	0.00372

The aperture ratio, f number, of mirror M_2 is 4.0, which is slightly larger than the f number of the spectrometer and thus acts as the limiting aperture for radiation incident on the collimator of the spectrometer.

There was some "noise" on the detector and amplifier system used to read out the signal from the spectrometer. To minimize the effect of this background noise, it was necessary to fill the collimator with as much radiation as possible in order for the signal from the detectors to be large compared to the noise level. This criterion was fulfilled by mirror M_4, since its f number was approximately the same as the f number of the collimator.

The requirement that aberrations should be kept to a minimum was the prime factor in determining the physical layout of the optics. The effect of aberrations in an optical system is to destroy the point-to-point correspondence between the object and the image. Without a point-to-point correspondence it would not have been possible to determine what area of the source the spectrometer was observing. In making intensity calibrations for the spectroscope, the area of the source being observed was needed; so, the optics system was designed to reduce aberrations to a minimum.

The six types of aberrations which can occur for a spherical mirror are chromatic aberrations, spherical aberrations, coma, astigmatism, curvature of field and distortion. A detailed discussion of each of these

aberrations has been given by Jenkins and White (10) and by Monk (11). Chromatic aberrations were eliminated by using only front silvered mirrors.

Spherical aberrations occur for spherically ground mirrors when the distance from the reflecting surface to the image is not equal for all points on the reflecting surface. The third order equation for the object distance is given by Morgan (12) as

$$\frac{1}{S'} = \frac{2}{R} - \frac{1}{S} + \left(\frac{1}{S} - \frac{1}{R}\right)^2 \frac{\rho^2}{R} \qquad (41)$$

where R is the radius of curvature of the mirror, ρ is the perpendicular distance from any point on the mirror to the line normal to the center of the mirror, S is the object distance, and S' is the image distance. For mirror M_2 the object distance was equal to the image distance, so the third term on the right-hand side was equal to zero and there was no spherical aberrations. For mirror M_3 equation 41 predicts a range of image distances of 18.0000 inches for ρ = 0 to 18.0076 for ρ = 2.5 inches, the outside radius of the mirror. This means that the image of a point source would be spread out along a line 0.0076 inches long rather than appearing at one point. This aberration was considered to have a negligible effect on the intensity calibrations.

The other types of distortion are caused by the image and the object being located off the line perpendicular to the center of the mirror. The theory of aberrations indicates that if the angle between the center

of the mirror and the image and the line perpendicular to the center of the mirror is small the aberrations will be small. If this angle is 3^{o} or less a sufficiently clear image will be produced. The optical system used for this experiment was designed for an angle of 3^{o}. Mirrors M_1, M_4 and M_5 were plane first-surface mirrors used to reflect the radiation through the large angles required to physically separate the sources, the flame holder, and the spectrometer.

The optical system was mounted on an aluminum slab 1/2 inch thick, 1-1/2 feet wide and 4-1/2 feet long which was bolted to a concrete slab table top 3 inches thick, 3-1/2 feet wide, and 6-1/2 feet long. The spectrometer sat on the concrete table top and was secured to the aluminum optical table. The mirror mounts were designed so that the line normal to the center of the mirrors could be adjusted to the height of the optical center line which was 4-1/4 inches above the top surface of the asluminum slab. The mirrors could be positioned in the correct direction by means of a three-point suspension which held the mirrors to the mirror mounts.

For mirror M_2 the object distance, S_2, and the image distance, S_2', were both 18 inches. The magnification of this mirror was unity so the area of the flame, A, observed by the spectrometer was equal to the width times the length of the spectrometer entrance slit. The solid angle (of the radiation emitted from the flame) that the optics intercepted and focused into the spectrometer was the area of mirror M_2 divided by

the object distance squared. Thus,

$$\Omega = \frac{\pi r^2}{(S_2)^2} = 0.04909 \qquad (42)$$

For mirror M_3 the object distance, S_3, was 28.29 inches and the image distance, S_3', was 18 inches, which gave a magnification M' of 0.636. Thus, the area of the source viewed by the spectrometer, A', was the width of the entrance slit divided by M' times the length of the slit divided by M'. The solid angle (of the radiation emitted by the source) which the optics intercepted and focused into the spectrometer, Ω', was given by

$$\Omega' = \frac{\pi r^2}{(S_3)^2} = 0.01988 \qquad (43)$$

Flame Holder and Boiler

Before spectral analysis could be performed on a flame, a method of producing a stable and reproducible flame was needed. The flames of interest were diffusion flames, but ordinary pan fires were too unstable for spectral analysis. A boiler was constructed to heat the fuel to a temperature corresponding to a vapor pressure of approximately 20 psi. The vapor was passed through a heated fuel line and expansion valve into a 2-1/2 inch tall burner made from a piece of 3/4 inch ID brass tubing. Two stainless steel screens were placed in the circular burner to straighten the flow and produce a steady laminar flow. This system was capable of producing a steady flame of constant size for

several hours. Figure 11 is a diagram of the flame holder and boiler system. The boiler, fuel line and flame holder were electrically heated by passing a current through a 20 gauge Nickel Chromium heater wire. The wire was insulated from the metallic surfaces by a layer of Sauereisen Electric Resistor Cement No. 78. Another layer of this cement and several layers of asbestos were used to insulate the entire heated system. The flame holder was mounted in a housing which allowed it to be moved in two directions. This allowed the spectrometer entrance slit to be focused onto several different locations on the flame.

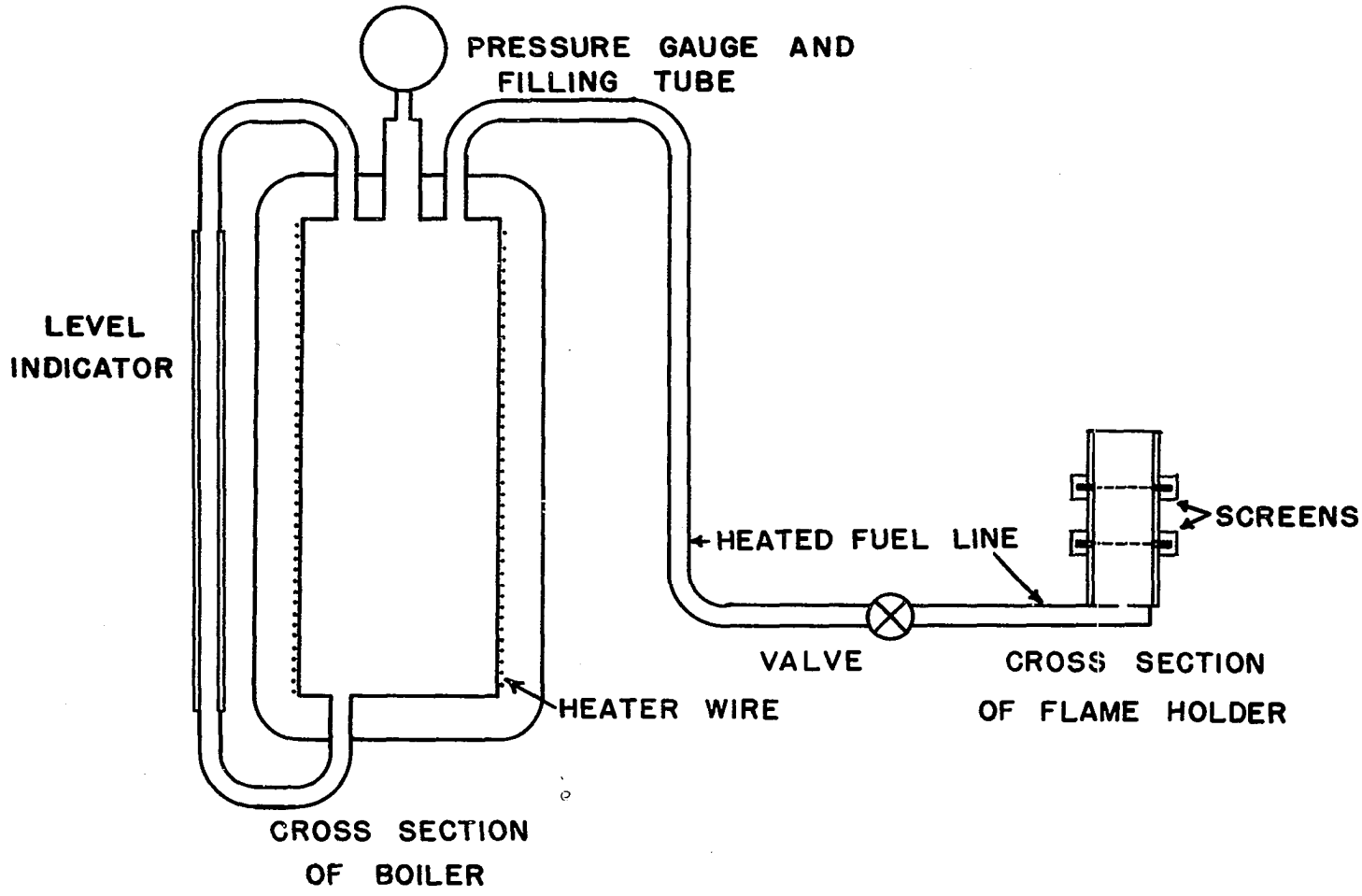


Figure 11. Diagram of Flame Holder and Boiler

CHAPTER III

CALIBRATIONS

The wavelength scanning mechanism for the Model 12-C spectrometer involves a motor-driven threaded shaft and a mechanical linkage which rotates the Littrow mirror. The wavelength drum is attached to the threaded shaft and indicates the position of the shaft. Wavelength calibrations involve determining the relationship between the wavelength drum settings and the wavelength. To do this several absorption peaks were identified and the corresponding wavelength drum settings determined. The wavelength of several absorption peaks of 1, 2, 4 trichlorobenzene, toluene, polystyrene, and didymium glass have been accurately determined by Plyler and his associates (3, 4, 5). A Perkin-Elmer Demountable Liquid Absorption Cell with NaCl windows was used to obtain the absorption data on the liquid samples. Table 2 is a list of the drum settings and absorption peak determined along with the sample observed and the reference from which the wavelength calibration was determined. Figure 12 is a graph of the wavelength versus wavelength drum settings for the wavelength region of 1.5 to 5.2 microns. Before each data run was started, a spectrogram of the absorption peaks of polystyrene was

TABLE II

WAVELENGTH DRUM CALIBRATION POINTS

Drum Setting	Wavelength in microns	Sample and calibration reference
2084.0	0.684	didymium glass
2050.5	0.743	shade 5
2018.5	0.808	Reference (4)
1937.0	1.067	
1920.0	1.22	
1806.0	3.3026	0.07 millimeter
1799.5	3.422	polystyrene film
1796.0	3.507	Reference (4)
1758.0	4.225	
1756.0	4.281	
1703.0	5.138	
1689.5	5.343	
1703.5	5.138	
1676.0	5.549	
1624.0	6.238	
1587.0	6.692	
1398.0	8.662	
1274.0	9.724	
1273.5	9.724	
1101.0	11.035	
1704.0	5.145	H_2O in atmosphere
1699.5	5.204	Reference (13)
1690.0	5.356	
1682.0	5.466	
1669.5	5.639	
1661.0	5.762	
1656.5	5.822	
1648.5	5.936	
1644.5	5.986	
1635.0	6.112	
1629.5	6.182	
1617.0	6.339	
1611.0	6.427	
1605.0	6.487	

TABLE II--Continued

Drum Setting	Wavelength in microns	Sample and calibration reference
1598.0	6.563	H_2O in atmosphere
1593.0	6.633	Reference (13)
1586.5	6.709	
1580.0	6.786	
1574.0	6.856	
1565.0	6.961	
1557.5	7.044	
1543.5	7.207	
1531.5	7.338	
1517.0	7.464	
1557	7.04	1, 2, 4 trichlorobenzene
1536.5	7.28	0.025 millimeter cell
1477.0	7.91	Reference (5)
1463.0	8.03	
1386.0	8.86	1, 2, 4 trichlorobenzene
1369.5	8.91	20:1 dilution in carbon
1343.5	9.14	disulfide 0.025 millimeter
1281.5	9.65	cell
914.5	12.27	Reference (6)
903.0	12.33	
1028.5	11.52	
914.5	12.27	
903.0	12.33	
1889.5	1.6606	1, 2, 4 trichlorobenzene
1859.7	2.1526	0.50 millimeter cell
1852.0	2.3126	Reference (5)
1847.8	2.403	
1846.3	2.4374	
1416	8.48	toluene 0.050 millimeter
1331	9.24	cell
1275.5	9.70	Reference (4)

TABLE II--Continued

Drum Setting	Wavelength in microns	Sample and calibration reference
1598.0	6.563	H_2O in atmosphere
1593.0	6.633	Reference (13)
1586.5	6.709	
1580.0	6.786	
1574.0	6.856	
1565.0	6.961	
1557.5	7.044	
1543.5	7.207	
1531.5	7.338	
1517.0	7.464	
1557	7.04	1, 2, 4 trichlorobenzene
1536.5	7.28	0.025 millimeter cell
1477.0	7.91	Reference (5)
1463.0	8.03	
1386.0	8.86	1, 2, 4 trichlorobenzene
1369.5	8.91	20:1 dilution in carbon
1343.5	9.14	disulfide 0.025 millimeter
1281.5	9.65	cell
914.5	12.27	Reference (6)
903.0	12.33	
1028.5	11.52	
914.5	12.27	
903.0	12.33	
1889.5	1.6606	1, 2, 4 trichlorobenzene
1859.7	2.1526	0.50 millimeter cell
1852.0	2.3126	Reference (5)
1847.8	2.403	
1846.3	2.4374	
1416	8.48	toluene 0.050 millimeter
1331	9.24	cell
1275.5	9.70	Reference (4)

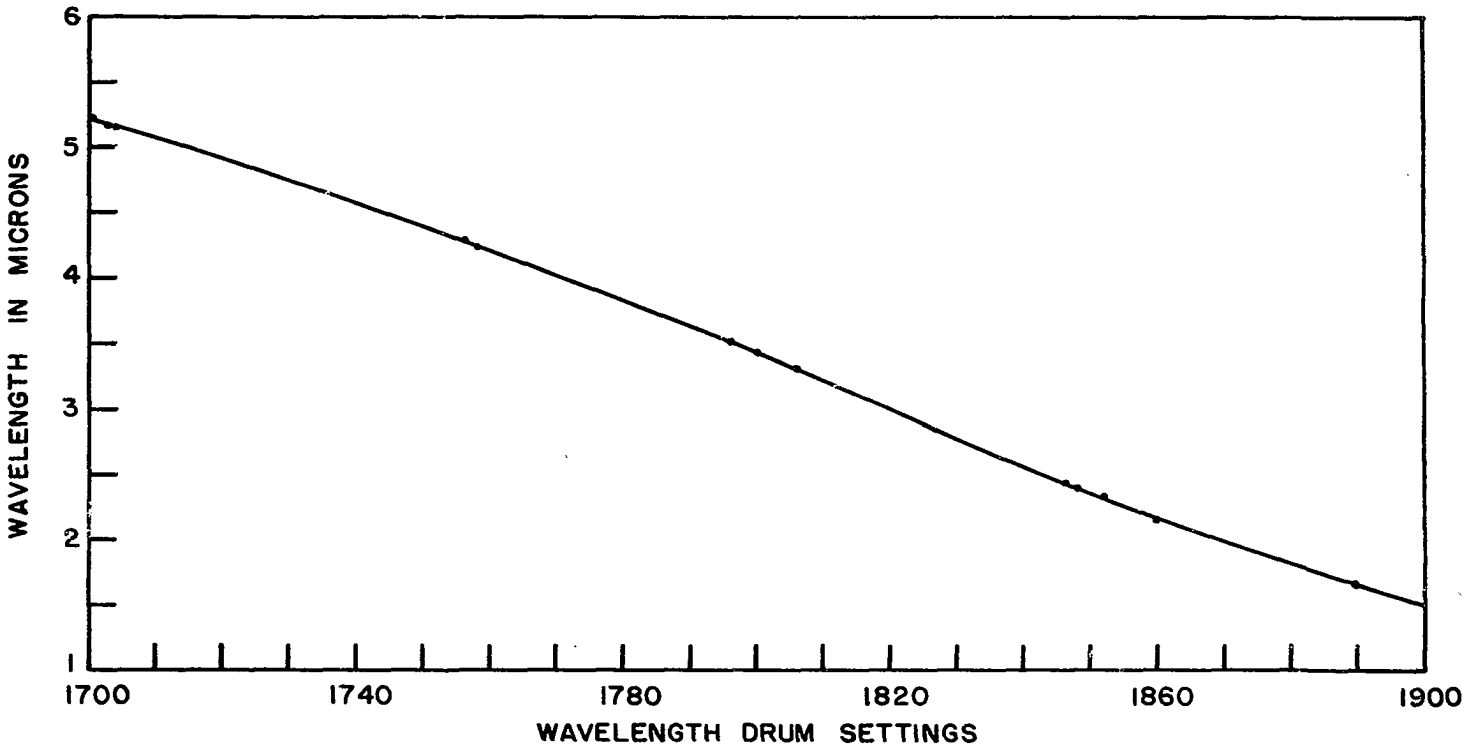


Figure 12. Wavelength Drum Settings versus Wavelength

taken to recheck the calibration. When this spectrogram did not agree with the wavelength calibration curve, the fine adjustment screw on the Littrow mirror was adjusted until they did agree. The reproducibility of the wavelength drum settings was checked by taking five consecutive spectrograms of the same absorption peak. The wavelength drum settings for the absorption peak all agreed within 1/100 of a revolution of the wavelength drum.

Absolute intensity calibrations of a spectrometer involve finding the relationship between the output of the radiation detector and the power incident on the detector in the spectrometer. The intensity emitted by a black body with emittance ϵ_λ is

$$I_\lambda = \frac{\epsilon_\lambda C_1}{\lambda^5} \left(\frac{1}{e^{C_2/\lambda T} - 1} \right) \tag{44}$$

where $C_1 = 1.177 \times 10^{-12}$ watts cm^2, $C_2 = 2.5776$ cm. degree Rankine, and λ is the wavelength in centimeters. From this expression the power incident on the detector of the spectrometer could be computed as

$$E_\lambda = \frac{\epsilon_\lambda A' C_1 \Omega'_\lambda}{\lambda^5} \left(\frac{1}{e^{C_2/\lambda T} - 1} \right) \tag{45}$$

where A', the area of the source being observed, was 1.236×10^{-2} cm; Ω', the solid angle collected by the optical system, was 1.988×10^{-2} steradians; and $\Delta\lambda$ was the wavelength interval being observed. The details of the calculations of $\Delta\lambda$ was covered in Chapter II Section 1 and the details of calculating A' and Ω' were given in Chapter II Section 2.

The two parameters necessary for completing this calculation are ϵ_λ and T.

The radiation source used for calibration purposes was a globar, a form of silicon carbide, 1/4 inch diameter and 2 inches long, which was electrically heated. The globar was purchased from the Perkin-Elmer Corporation. The temperature of the globar was measured by inserting a Chromel Alumel thermocouple into a 0.052 inch diameter hole drilled in it. In order to reduce the effect of heat loss along the thermocouple leads, the hole was drilled to a depth of 7/8 of the diameter of the globar thus embedding the thermocouple close to the surface with the leads coming out the other side. The leads were insulated with Sauereisen Electric Resistor Cement No. 78 to further reduce the effect of heat loss through the thermocouple leads. The radial temperature drop in the globar was estimated from the formula

$$T_r = \frac{\dot{q}\, r^2}{4\, k} \tag{46}$$

where $\dot{q}$ is the power dissipated per unit volume, r is the radius, and k is the thermal conductivity. For a globar temperature of 800°F which was the usual temperature during data runs, k = 22 BTU per hour foot degree Fahrenheit and T_r, the radial temperature difference, was approximately 2°F, which was negligible for this experiment. The temperature of the globar was recorded using ice-bath reference junctions and a chart recorded. An amplifier with a zero offset was used as an

input to the chart recorder so a $1^{o}R$ change of a $1500^{o}R$ temperature could be detected. The amplifier and recorder were calibrated before each data run using a Leeds and Northrup Co. Millivolt Potentiometer Cat. No. 8686.

The emittance of a globar radiation source has been discussed in detail by J. C. Morris (14). From his measurements and some other measurements on which he has made some corrections, it appears that an emittance of 0.93 can be used for the spectral region 1 to 6 microns with only one to 2 percent error. Also the comparison of the temperature measured with the thermocouple and the color temperature determined from a Pyro Micro-Optical Pyrometer Serial No. M-5438 gave an emittance of 0.93. Thus, this value was assumed for our calibrations. The intensity calibrations involve taking a spectrogram of the intensity radiated from the globar simultaneously with its temperature record. The black body intensity was computed and multiplied by an emittance of 0.93 for the three wavelengths of 2.18, 3.82, and 4.70 microns. These three wavelengths were chosen because they are in regions which are free from atmospheric absorption. The intensities computed for these 3 wavelengths were divided by the deflection on the spectrogram corresponding to the same wavelengths to determine the full scale intensity for the recorder. The three full-scale intensities so determined typically had less than 1 percent mean deviation. This method of data reduction also allowed a check on the gray body assumption: since once

the full scale deflection intensity and the temperature were known, the emittance for any wavelength could be computed. With the exception of the atmospheric absorption peaks the values of emittance thus computed were within 2 percent of the 0.93 value assumed. Thus, it was assumed that absolute intensity calibrations could be made with an error of less than 3 percent by assuming a gray body emittance of 0.93 and determining the globar temperature with a thermocouple placed in the manner described above.

In the discussion of equations 20 and 21 it was pointed out that an error was introduced by using equation 21, based on the mean value theorem, for the total integrated intensity rather than using equation 20. A numerical analysis was performed to estimate whether or not using equation 21 introduced an appreciable error for the intensity calibrations. To do this, the following fact was used: the mean value theorem of integration and the trapezoidal rule for integration give values which bracket the value for the integral of the function within some interval if there is no inflection point or discontinuity in the function within the interval. The value given by the trapezoidal rule, T, for the integral of the function f(x) in the interval b-a is

$$T = (b-a)\left[\frac{f(a) + f(b)}{2}\right] \tag{47}$$

and the value given by the mean value rule, M, for the integral of the function f(x) in the interval b-a is

$$M = (b-a)\, f\left(\frac{a+b}{2}\right) \tag{48}$$

For a function with a negative second derivative

$$T < \int_a^b f(x)\, dx < M \tag{49}$$

and for a function with a positive second derivative

$$T > \int_a^b f(x)\, dx > M \tag{50}$$

Thus, if the difference between the values computed by the mean value rule and the trapezoidal rule are negligible it can be assumed that the error introduced by using the mean value rule for the actual integrated value will be negligible for the function with no discontinuities or inflection points within the interval. Table 3 presents the results of calculations for the integrated intensity of a black body at 2160° K over the slit width interval $\Delta\lambda$ used this experiment, where

$$T = 2\Delta\lambda \ \frac{I_\lambda(\lambda_0 + \Delta\lambda) + I_\lambda(\lambda_0 - \Delta\lambda)}{2} \tag{51}$$

$$M = 2\Delta\lambda I_\lambda(\lambda_0) \tag{52}$$

and

$$\% \text{ error} = \frac{2|M - T|}{M + T} \times 100 \tag{53}$$

Since the spectrometer views intensity over the interval $\lambda_0 - \Delta\lambda$ to

$\lambda_0 + \Delta\lambda$, it can be seen that the percent of error is negligible for $\lambda > 1.5$ and the much simpler equation 21 can be used rather than equation 20 without introducing any appreciable error.

TABLE III

INTEGRATION ERROR ANALYSIS

λ	$\Delta\lambda$	T	M	% Error
1.00	0.0095	1.51307×10^{1}	1.46926×10^{1}	0.29
1.50	0.0280	3.04348×10^{2}	3.04378×10^{2}	0.0001
2.00	0.0488	9.20952×10^{2}	9.22053×10^{2}	0.0017
2.50	0.0596			
3.00	0.0624	1.15318×10^{3}	1.15337×10^{3}	0.0001
3.50	0.0602	9.22520×10^{2}	9.21953×10^{2}	0.0006
4.00	0.0565	6.95770×10^{2}	6.95888×10^{2}	0.0002
4.50	0.0525	5.08405×10^{2}	5.09150×10^{2}	0.0015
5.00	0.0491	3.74731×10^{2}	3.74323×10^{2}	0.0011
5.50	0.0460	2.77443×10^{2}	2.77323×10^{2}	0.0004
6.00	0.0431	2.06904×10^{2}	2.06833×10^{2}	0.0003

CHAPTER IV

ANALYSIS OF DATA

After the calibrations of wavelength were made and the full-scale intensity for each amplifier gain used was determined, the data reduction became a matter of reading values from the spectrographs of the flame itself, and the flame with the globar radiation incident on it and reading values from the temperature charts for corresponding wave-drum settings. These data were fed into a computer program which converted the data into intensity versus wavelength information and then performed the computations indicated by equations 10 and 8 to obtain values for J_λ and β_λ. Figures 13-24 show these data for several positions on an acetone and a methanol flame. Figure 25 gives the coordinate system used for the flame. The area of the flame observed was 0.100 millimeters in width by 5 millimeters in height. The y-z positions are the distance from the center of the coordinate system to the center of the bottom of the area being observed. The graphs for acetone show that J_λ and β_λ are approximately the same for all positions except for the bottom row ($z = 0$). A picture of the acetone flame showed a gap of approximately 1/8 inch between the flame holder and the luminous base

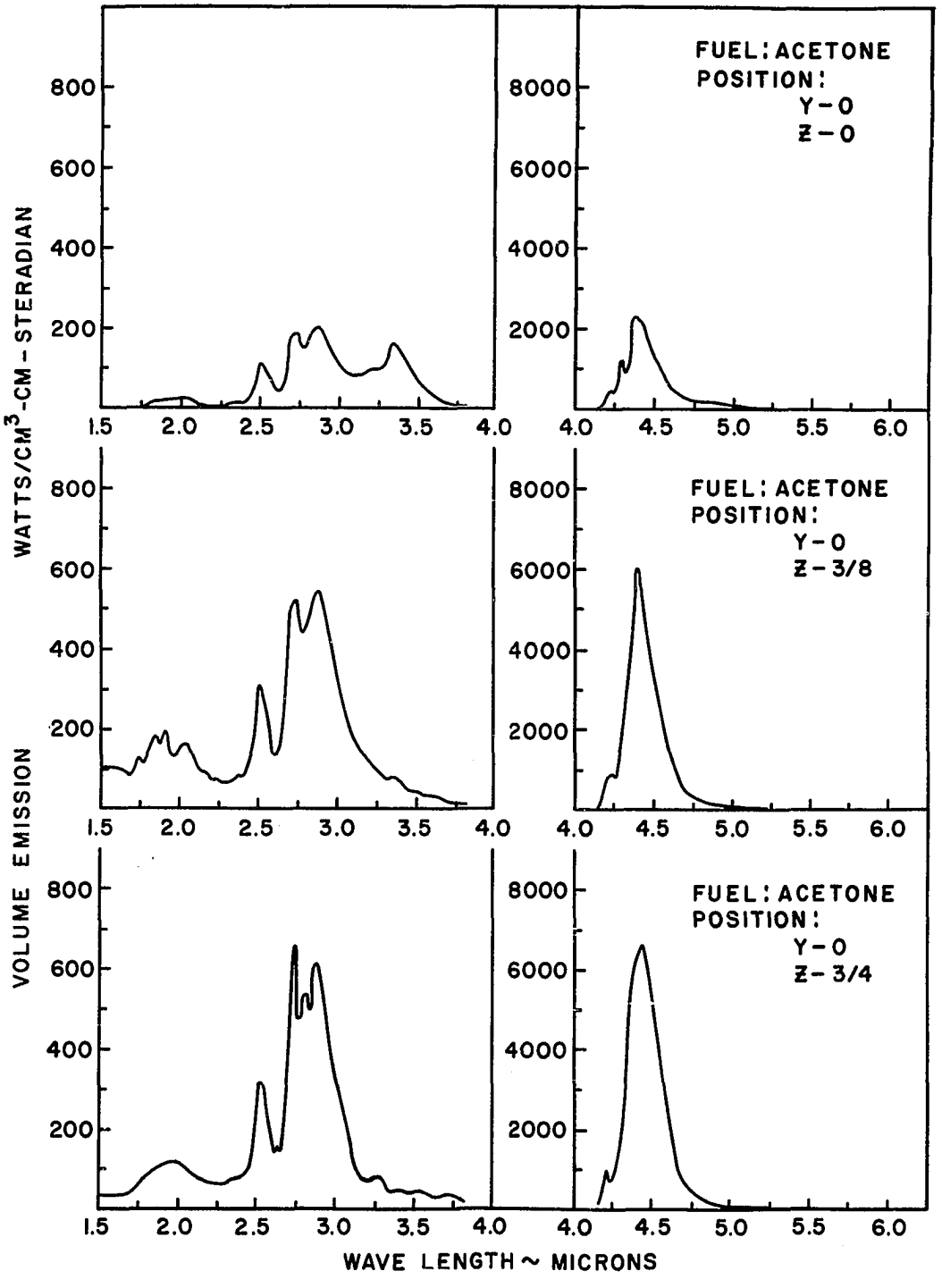


Figure 13. Acetone Flame Volume Emission (Y = 0)

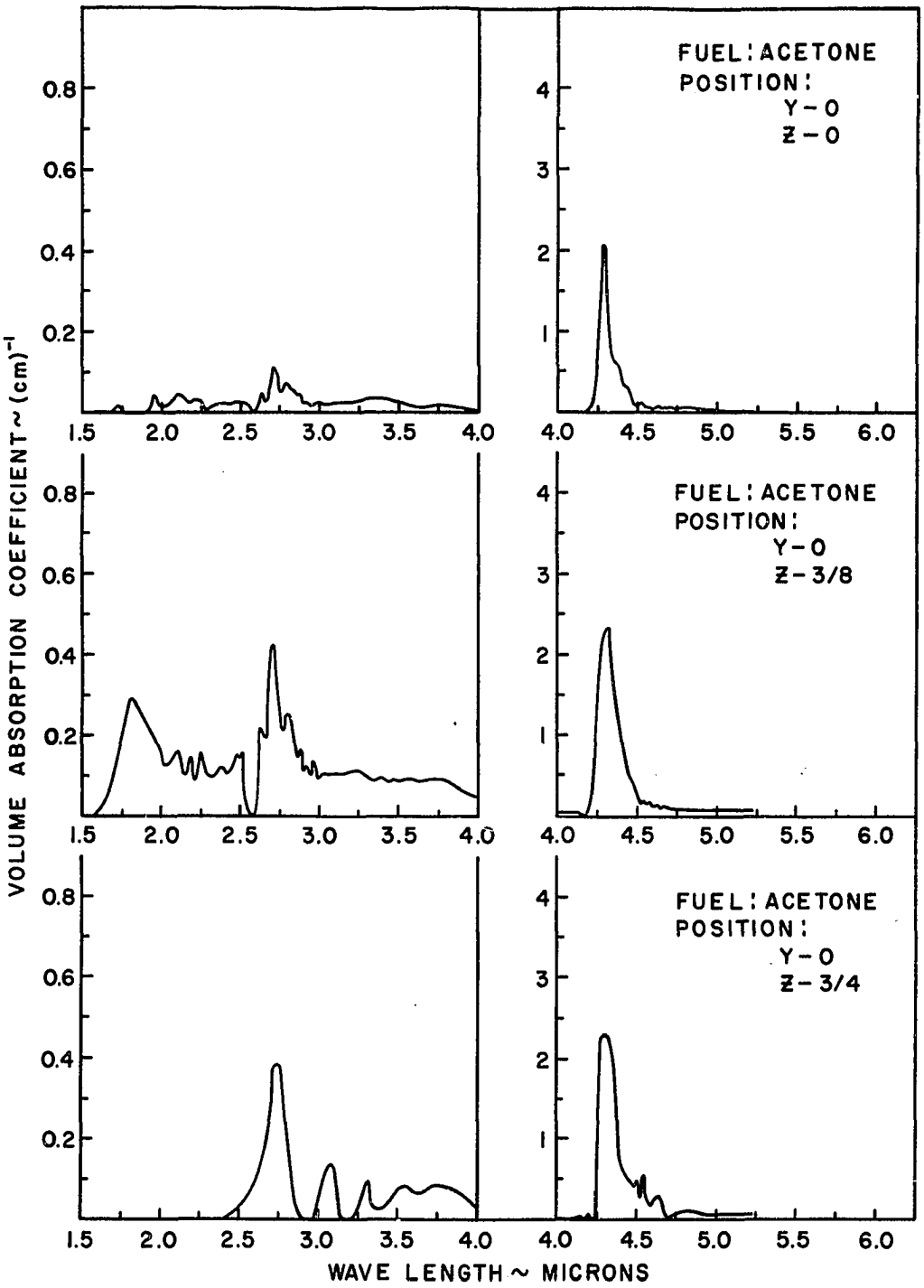


Figure 14. Acetone Flame Volume Absorption Coefficient (Y = 0)

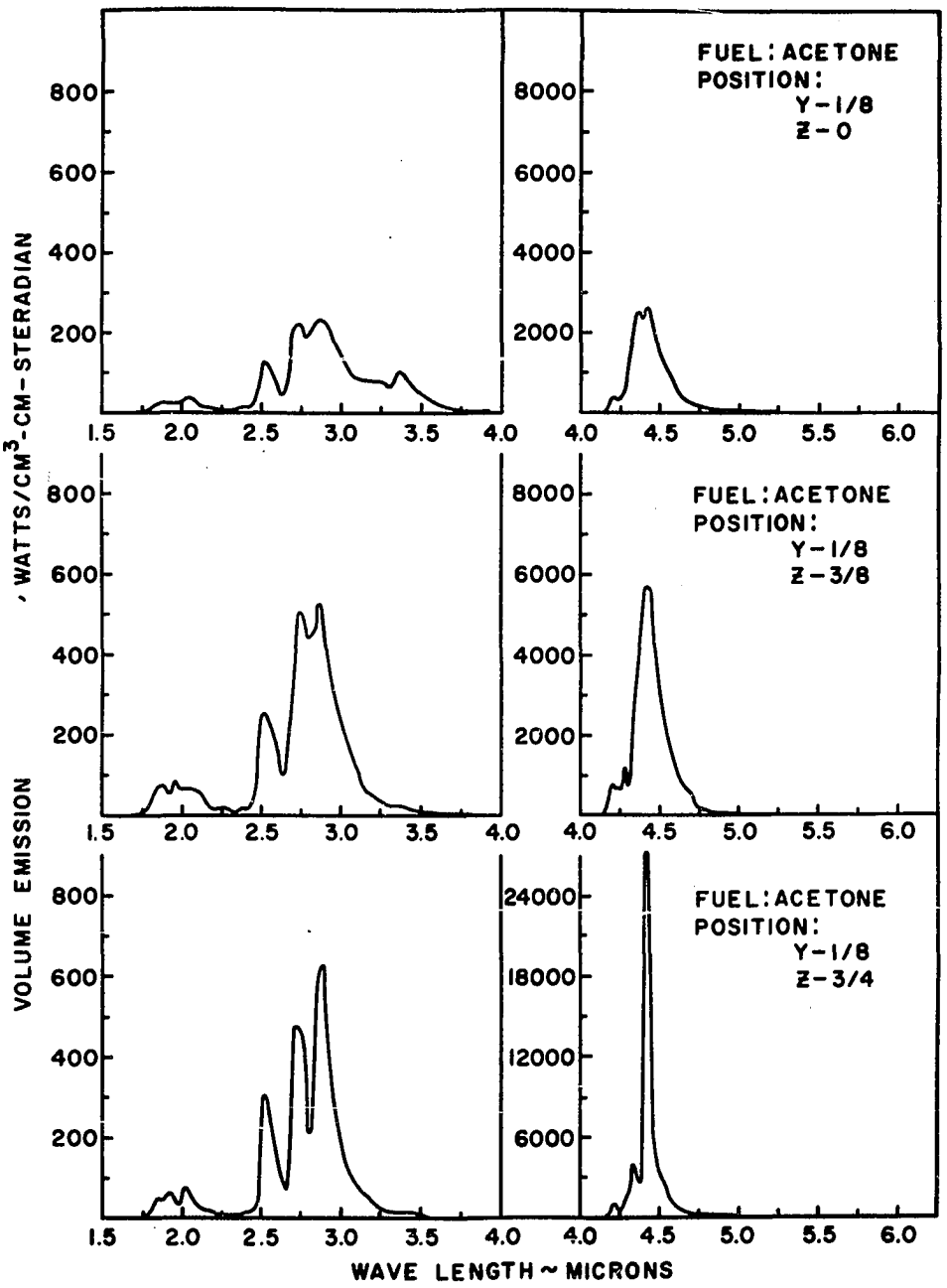


Figure 15. Acetone Flame Volume Emission (Y = 1/8)

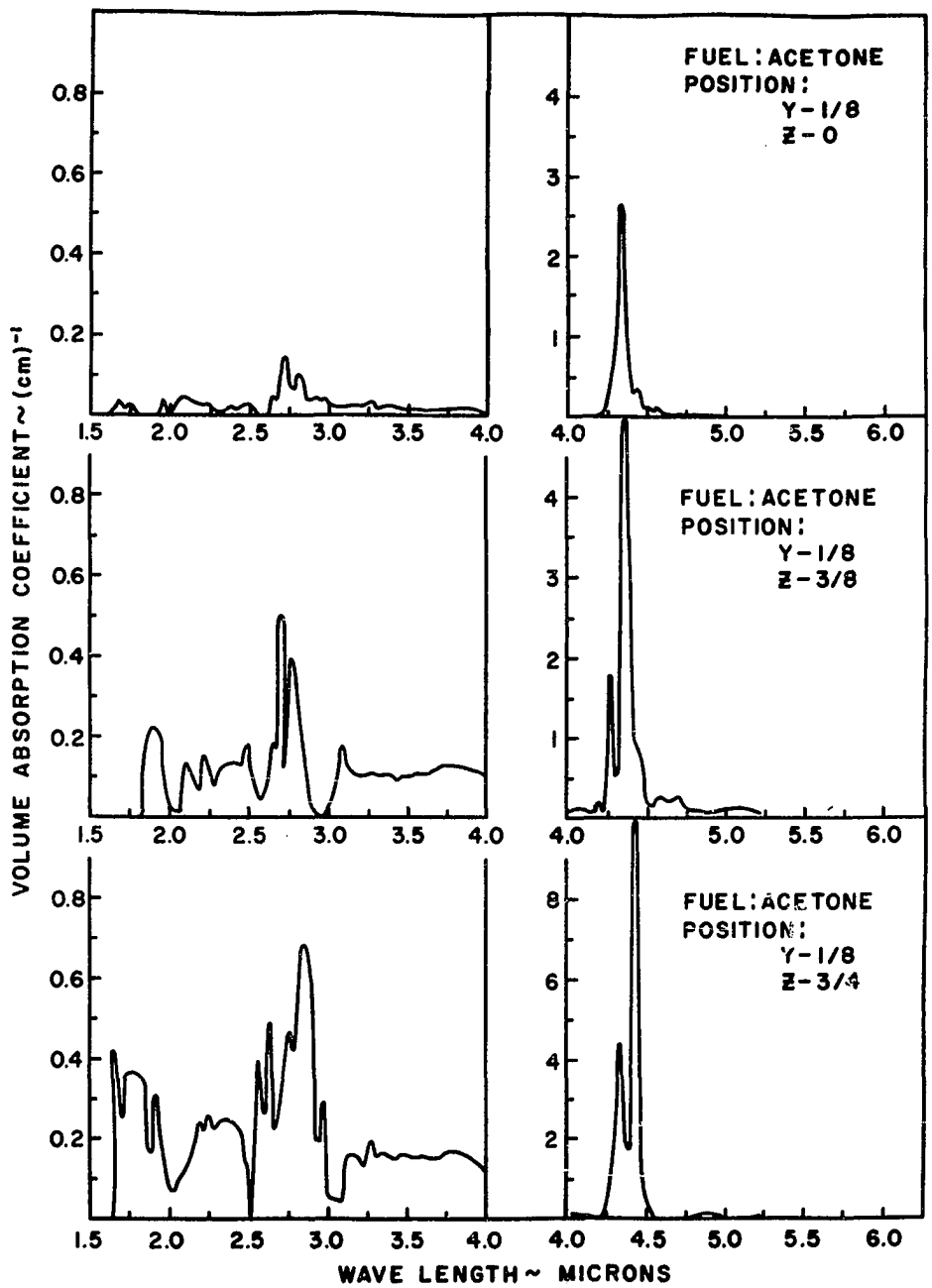


Figure 16. Acetone Flame Volume Absorption Coefficient (Y = 1/8)

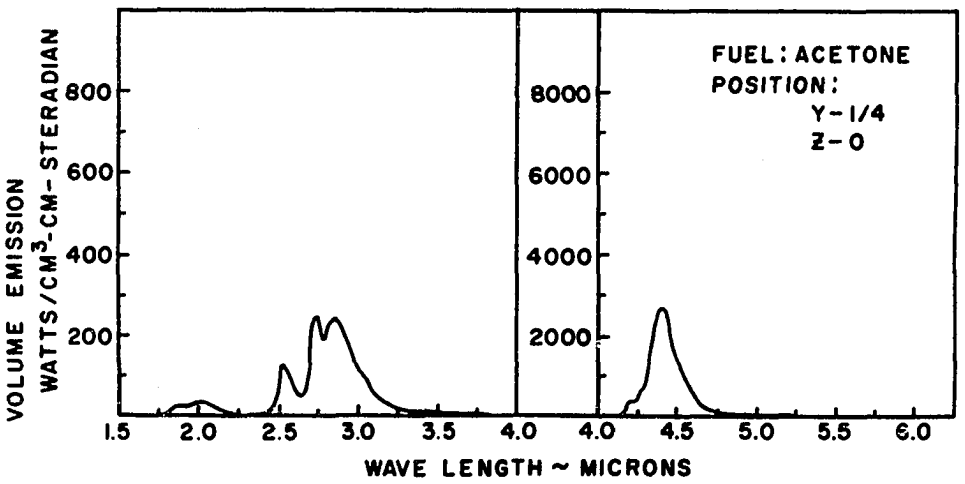


Figure 17. Acetone Flame Volume Emission (Y = 1/4)

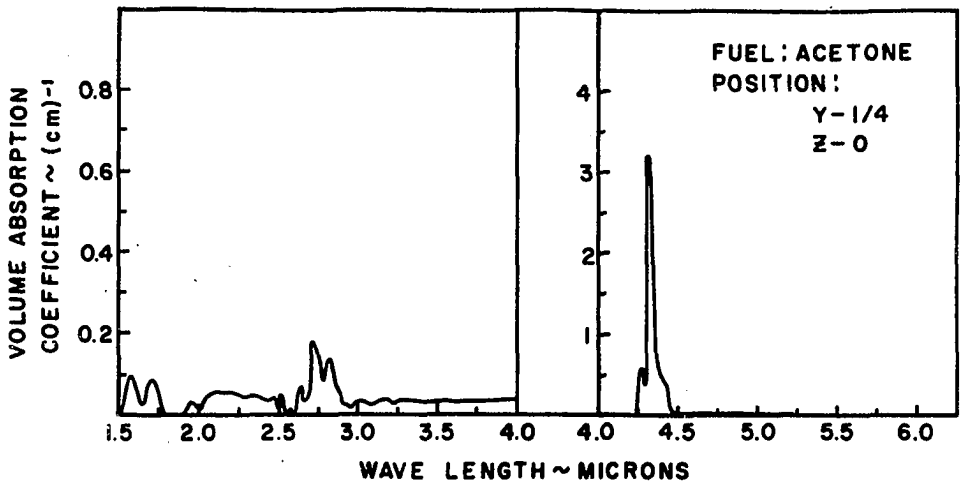


Figure 18. Acetone Flame Volume Absorption Coefficient (Y = 1/4)

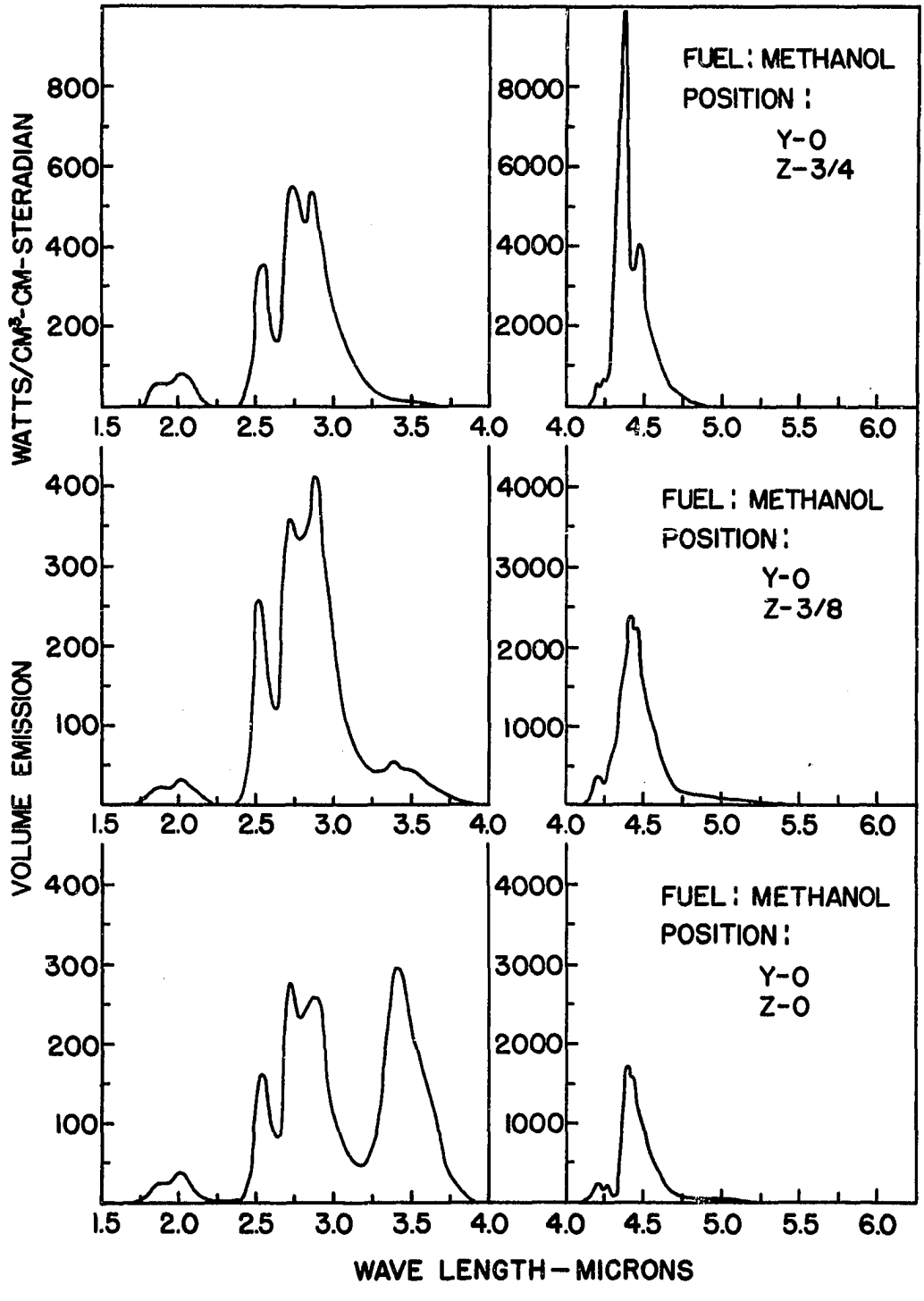


Figure 19. Methanol Flame Volume Emission (Y = 0)

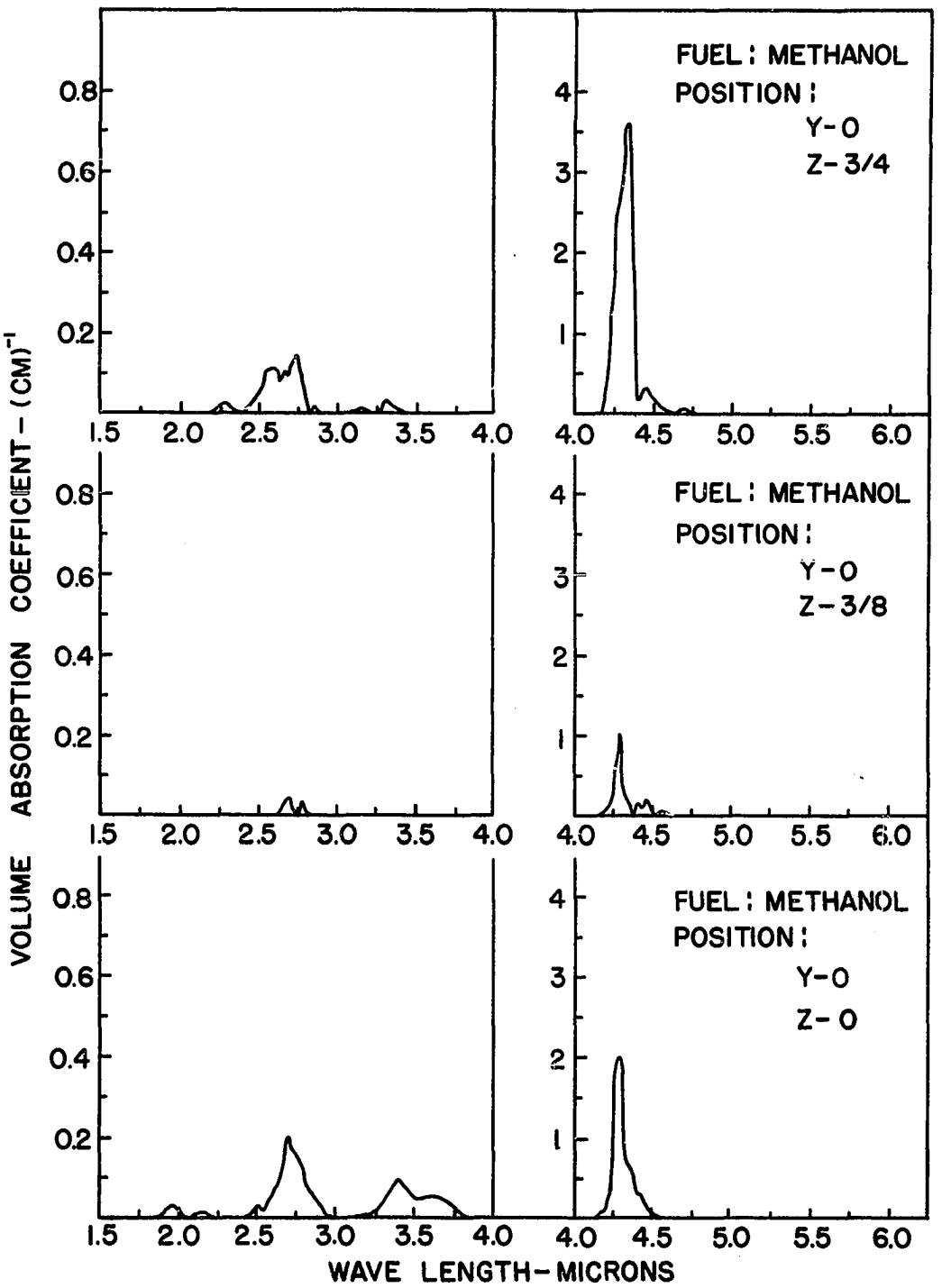


Figure 20. Methanol Flame Volume Absorption Coefficient (Y = 0)

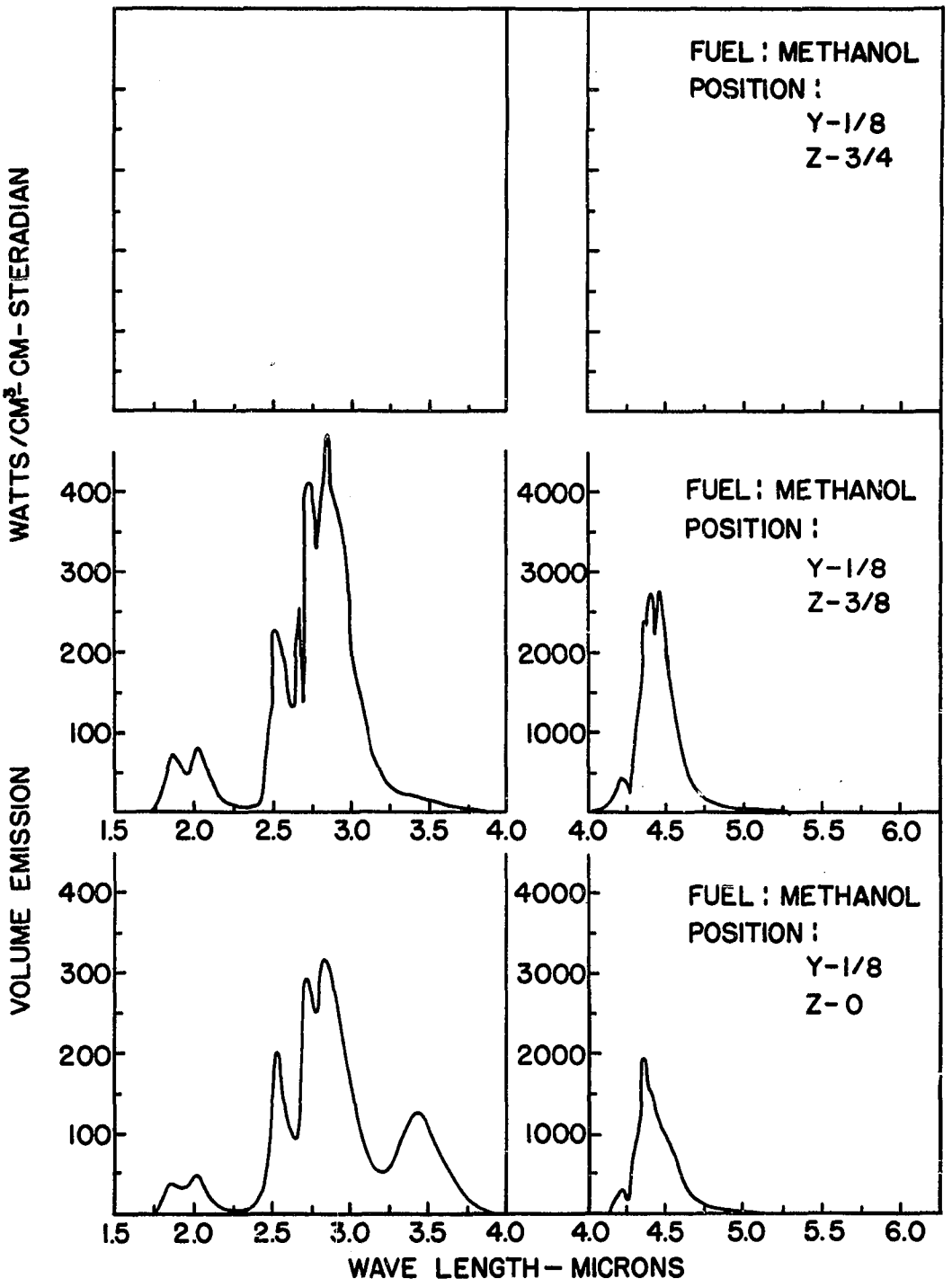


Figure 21. Methanol Flame Volume Emission (Y - 1/8)

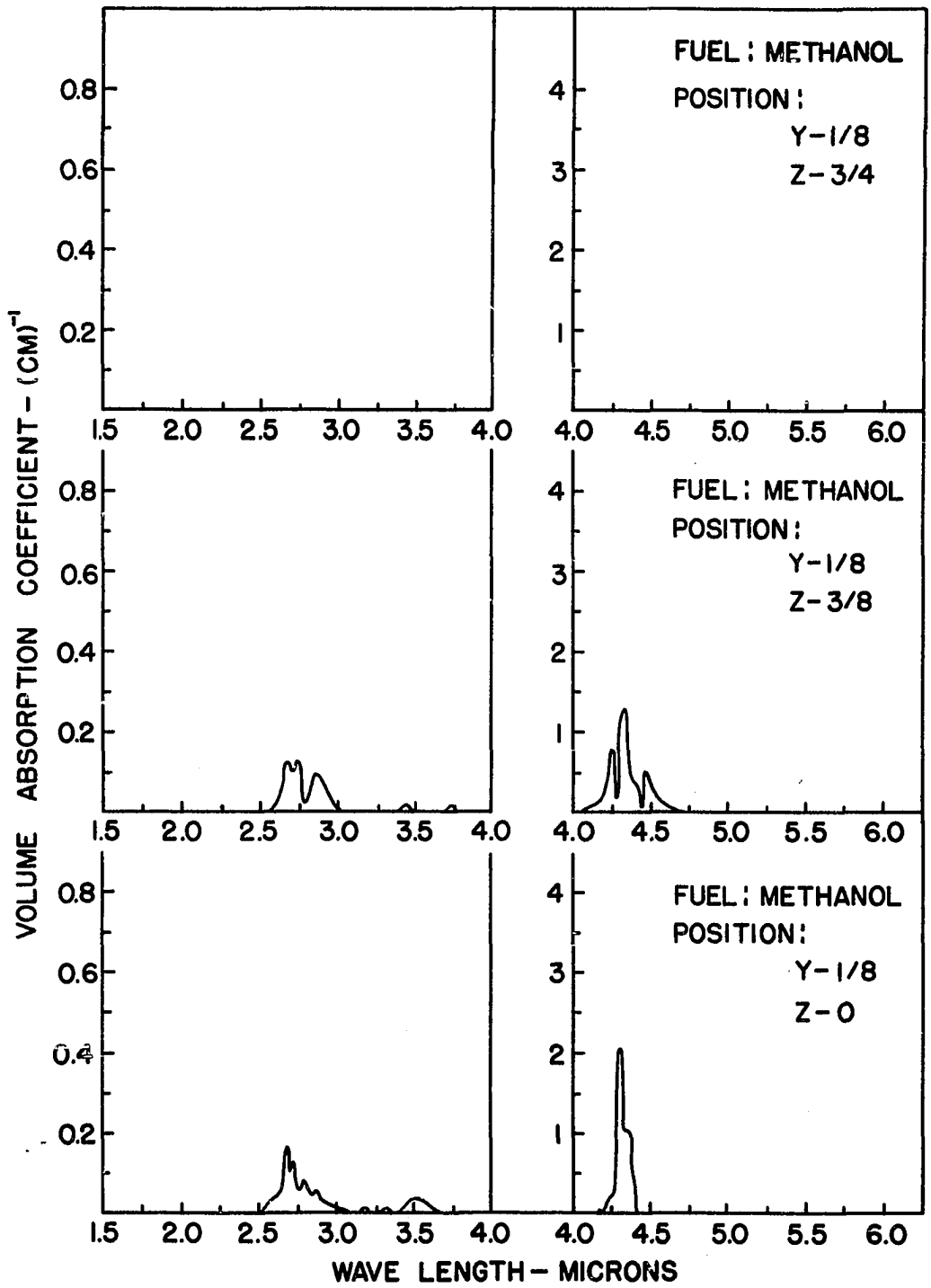


Figure 22. Methanol Flame Volume Absorption Coefficient (Y = 1/8)

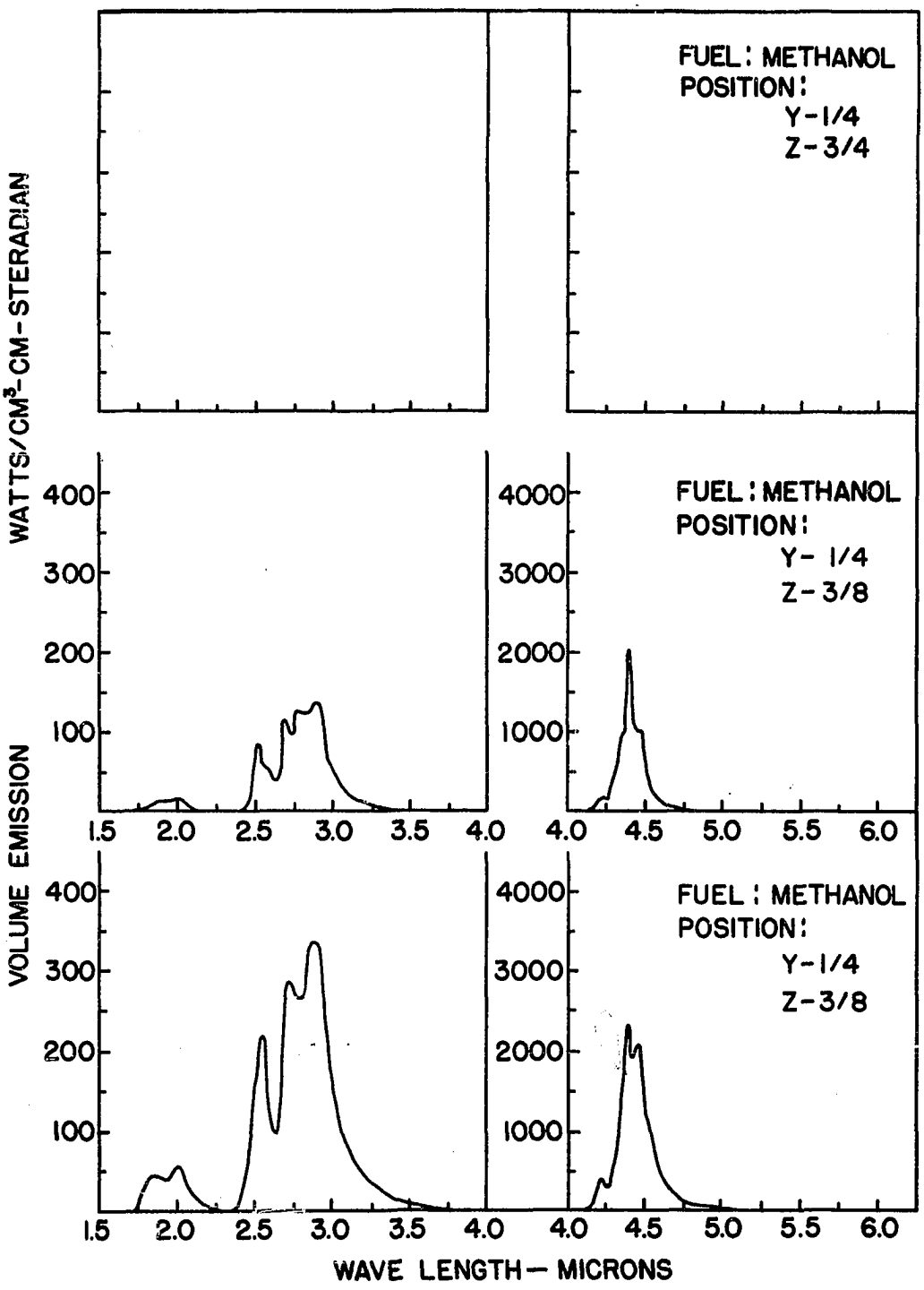


Figure 23. Methanol Flame Volume Emission (Y = 1/4)

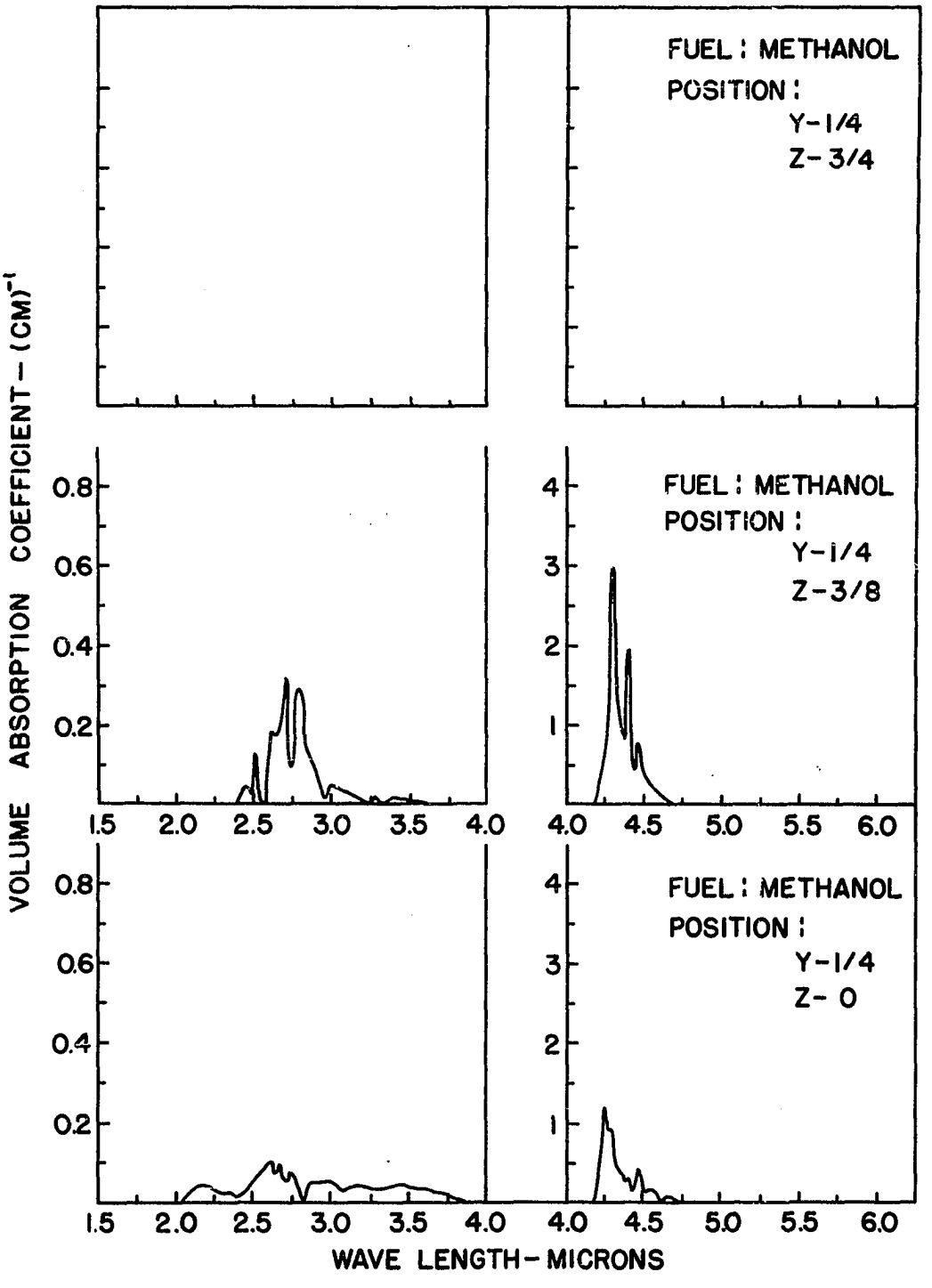


Figure 24. Methanol Flame Volume Absorption Coefficient (Y = 1/4)

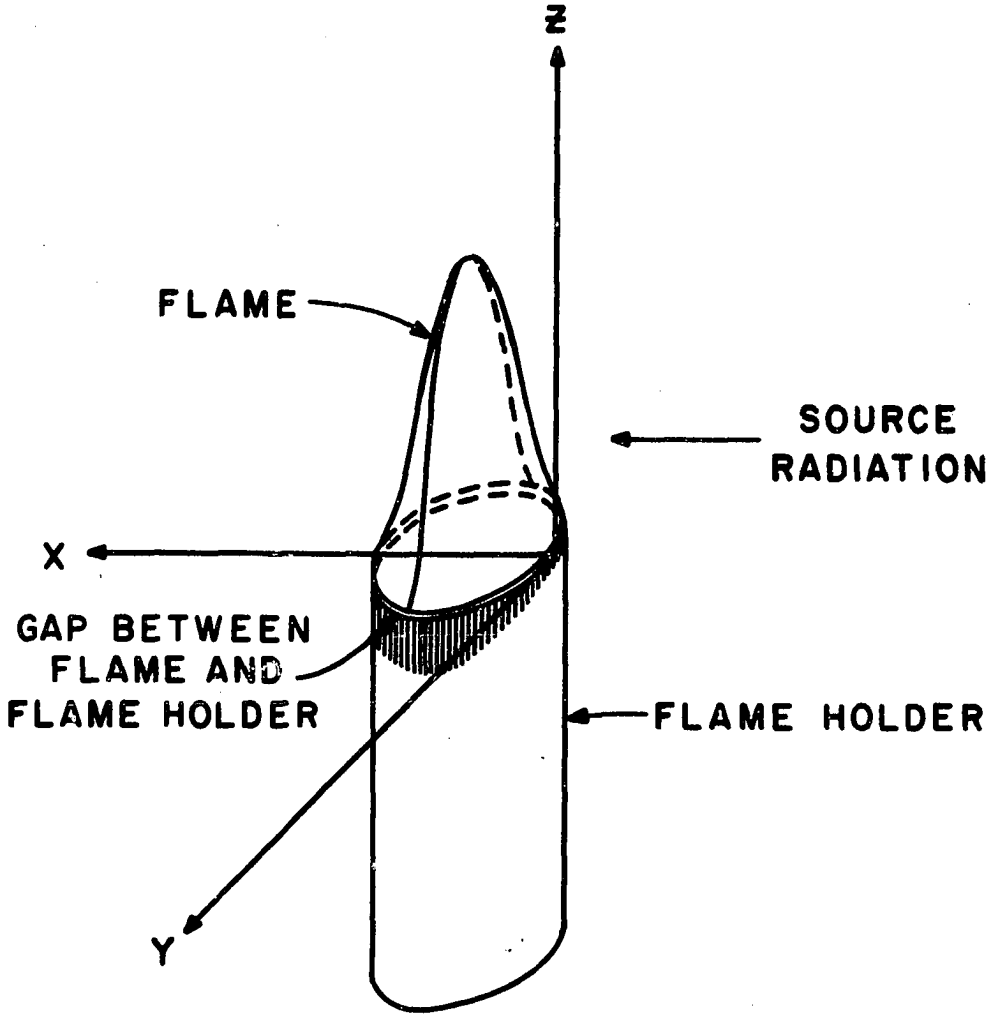


Figure 25. Coordinate System for Flames

of the flame which explained why the J_λ and β_λ are lower for the bottom row of graphs. This gap did not occur on the methanol flame, and it can be seen that J_λ was essentially independent of position. A flame 1-1/8 inches tall and 3/4 inch in diameter at the base was used for both the acetone and the methanol flames. The graphs indicate that the use of a lumped system parameter for J_λ and β_λ was a quite reasonable assumption for acetone and methanol. The values of J_λ and β_λ were used in equation (7) to compute the intensity for several values of x. It can be observed in Figures 26, 27 that for large diameter flames the intensity becomes independent of the diameter. This would be expected since as the diameter increases the flame becomes optically thick and starts emitting in the manner of a solid object. As this occurs the continuum intensity approaches a black body curve. However, the large CO_2 peak always was present which caused an error in the total flux when only the continuum radiation was accounted for.

Figures 28-35 are the J_λ and β_λ for several positions on the cyclohexane and n-hexane flames. The outer cone of these flames contained a much larger amount of carbon particles than the acetone and methanol flames. The spectrograms of the cyclohexane and n-hexane flames taken near their bases ($z = 0$) are very similar to the spectrograms of the methanol and acetone flames. The spectrograms taken of the flames 3/8 inch and 3/4 inch above the base of the flames are quite different due to the presence of the hot carbon particles. These

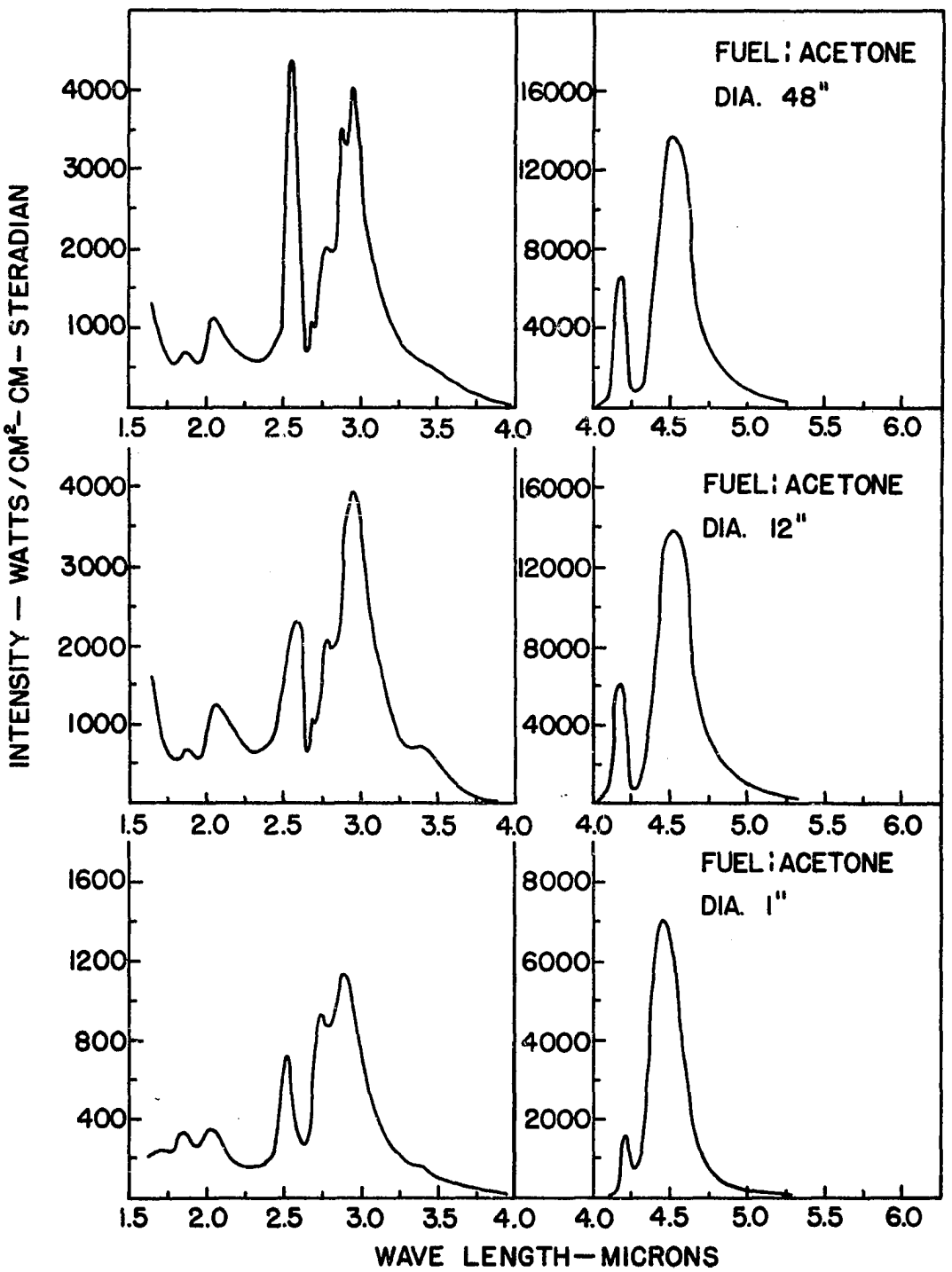


Figure 26. Acetone Flame Extrapolation

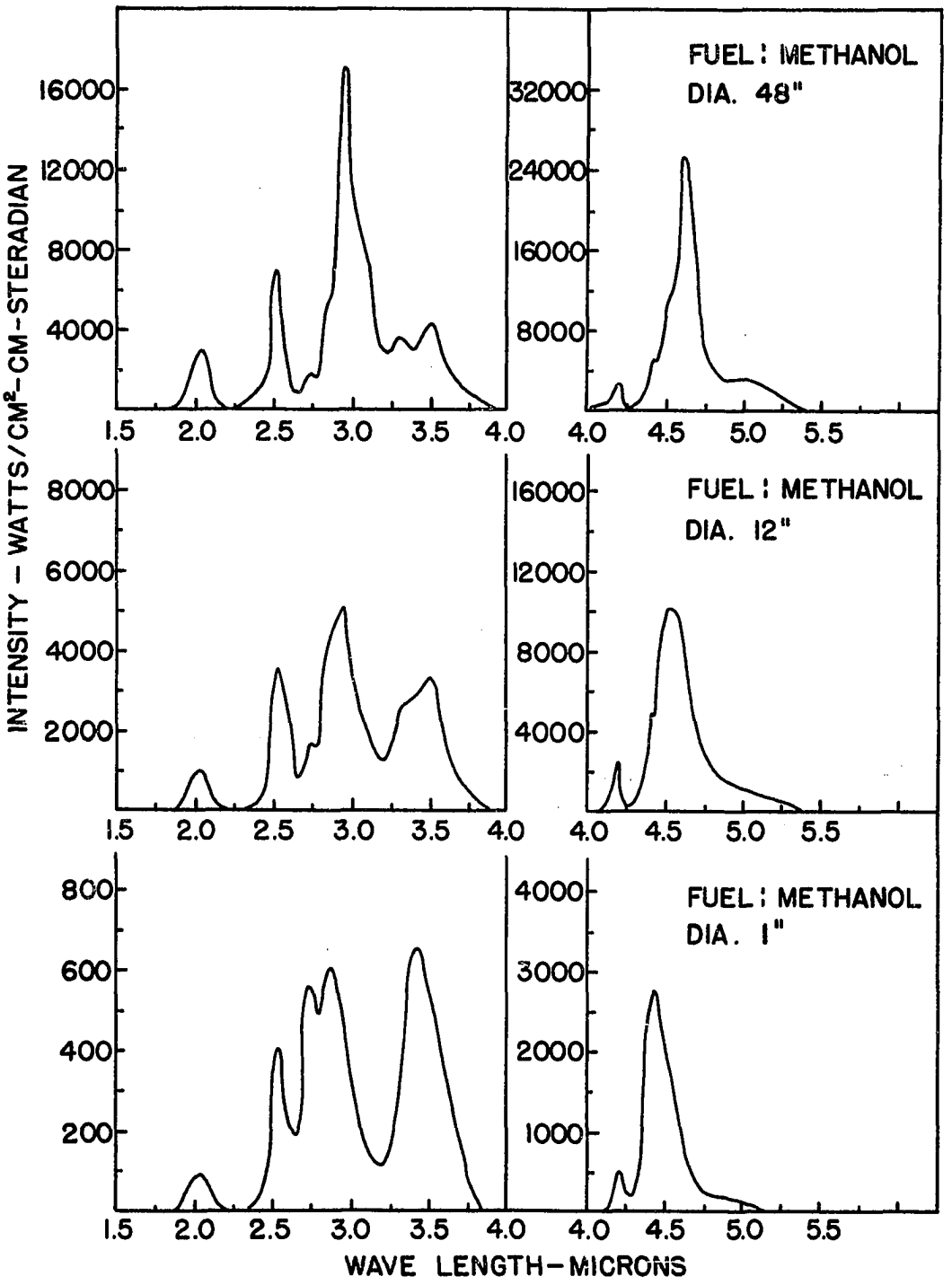


Figure 27. Methanol Flame Extrapolation

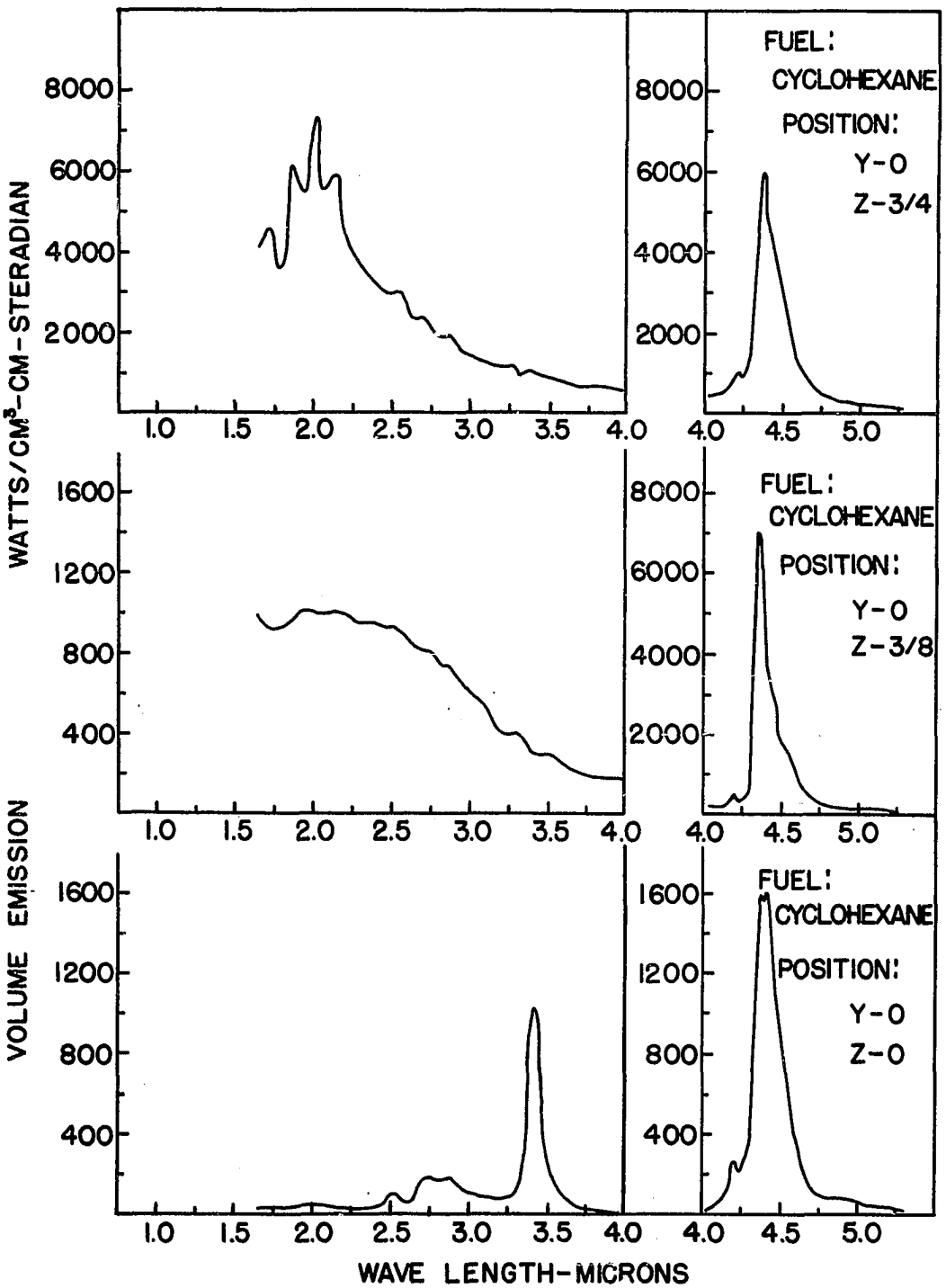


Figure 28. Cyclohexane Flame Volume Emission (Y = 0)

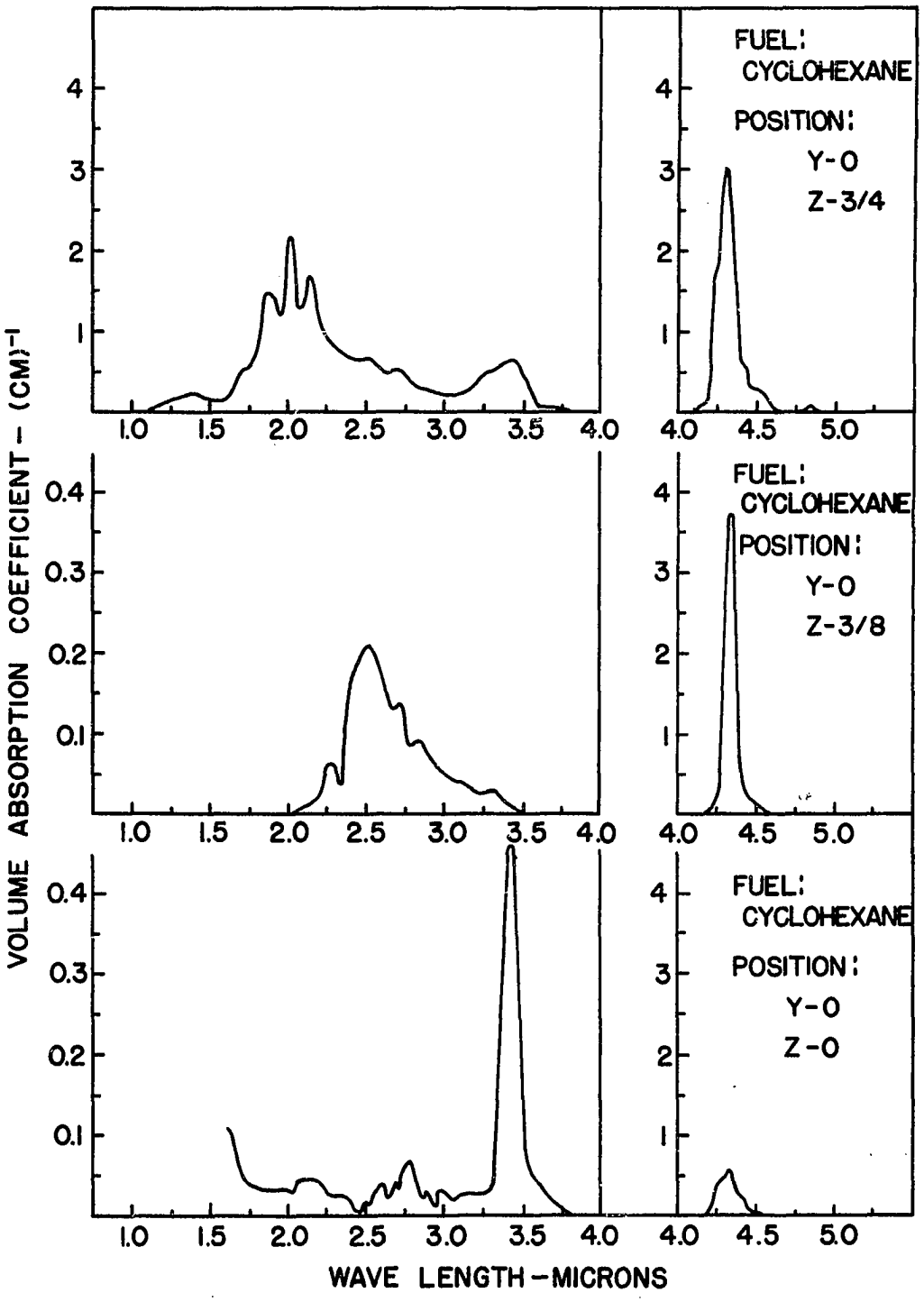


Figure 29. Cyclohexane Flame Volume Absorption Coefficient (Y = 0)

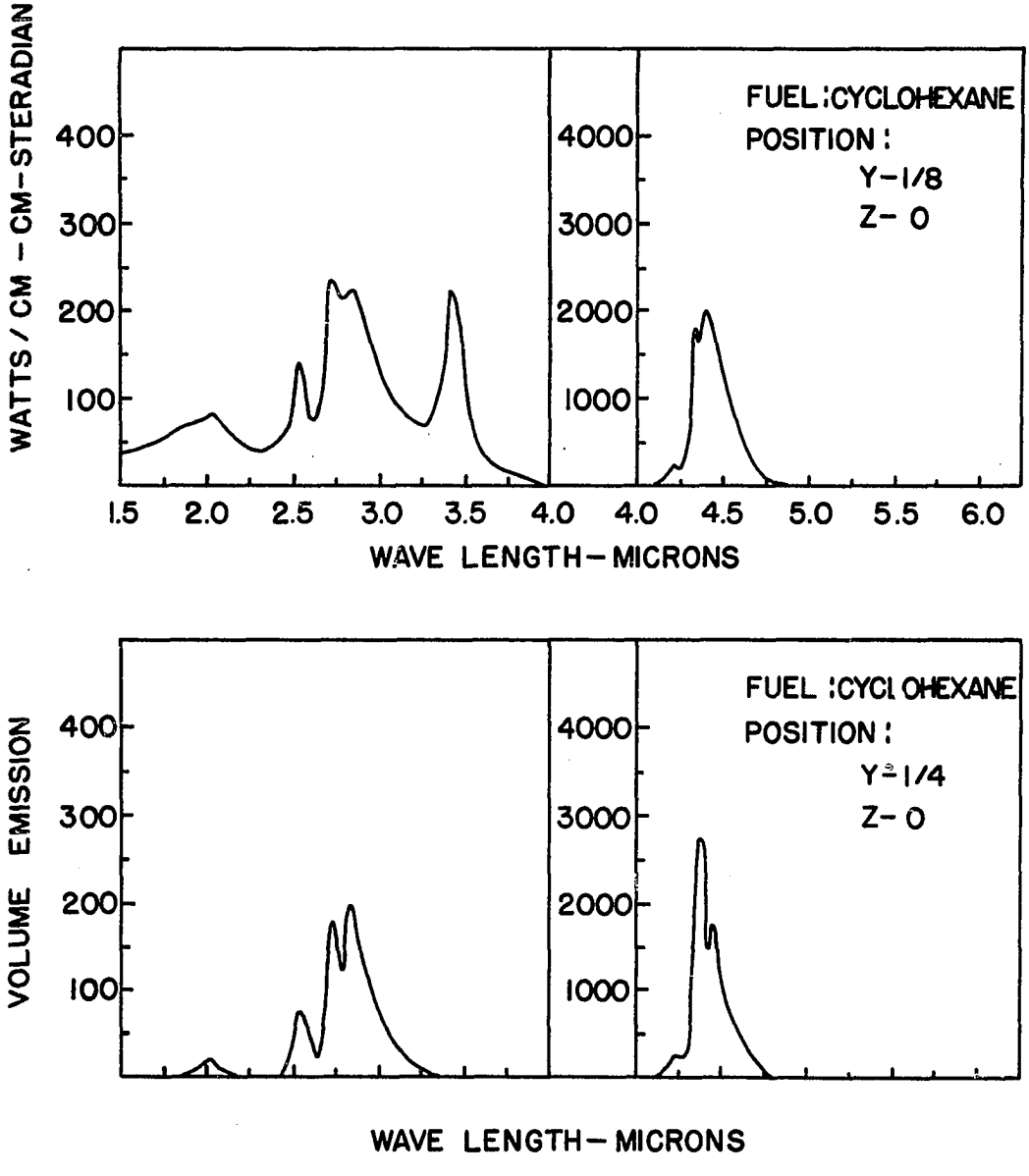


Figure 30. Cyclohexane Flame Volume Emission (z = 0)

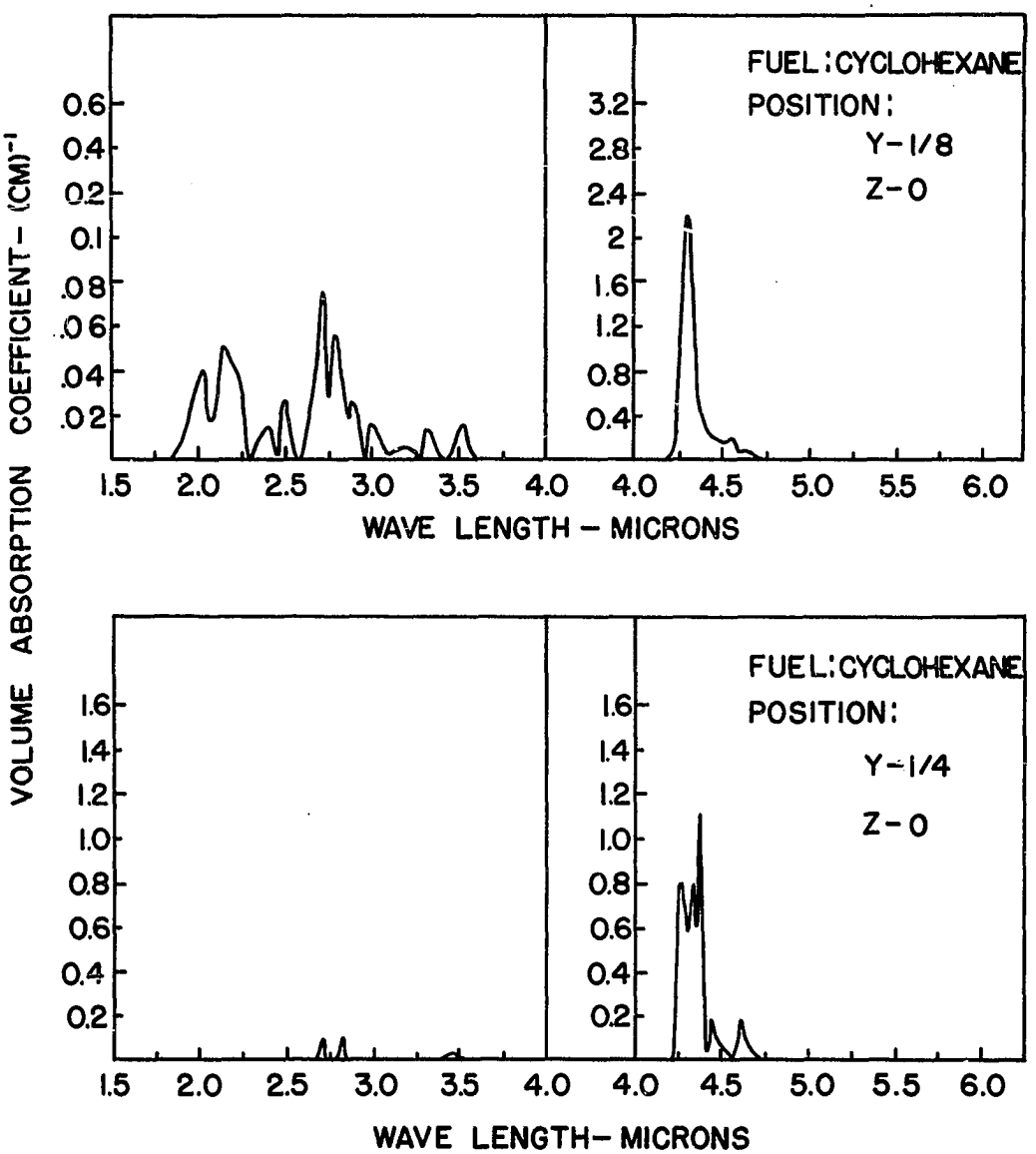


Figure 31. Cyclohexane Flame Volume Absorption Coefficient (z = 0)

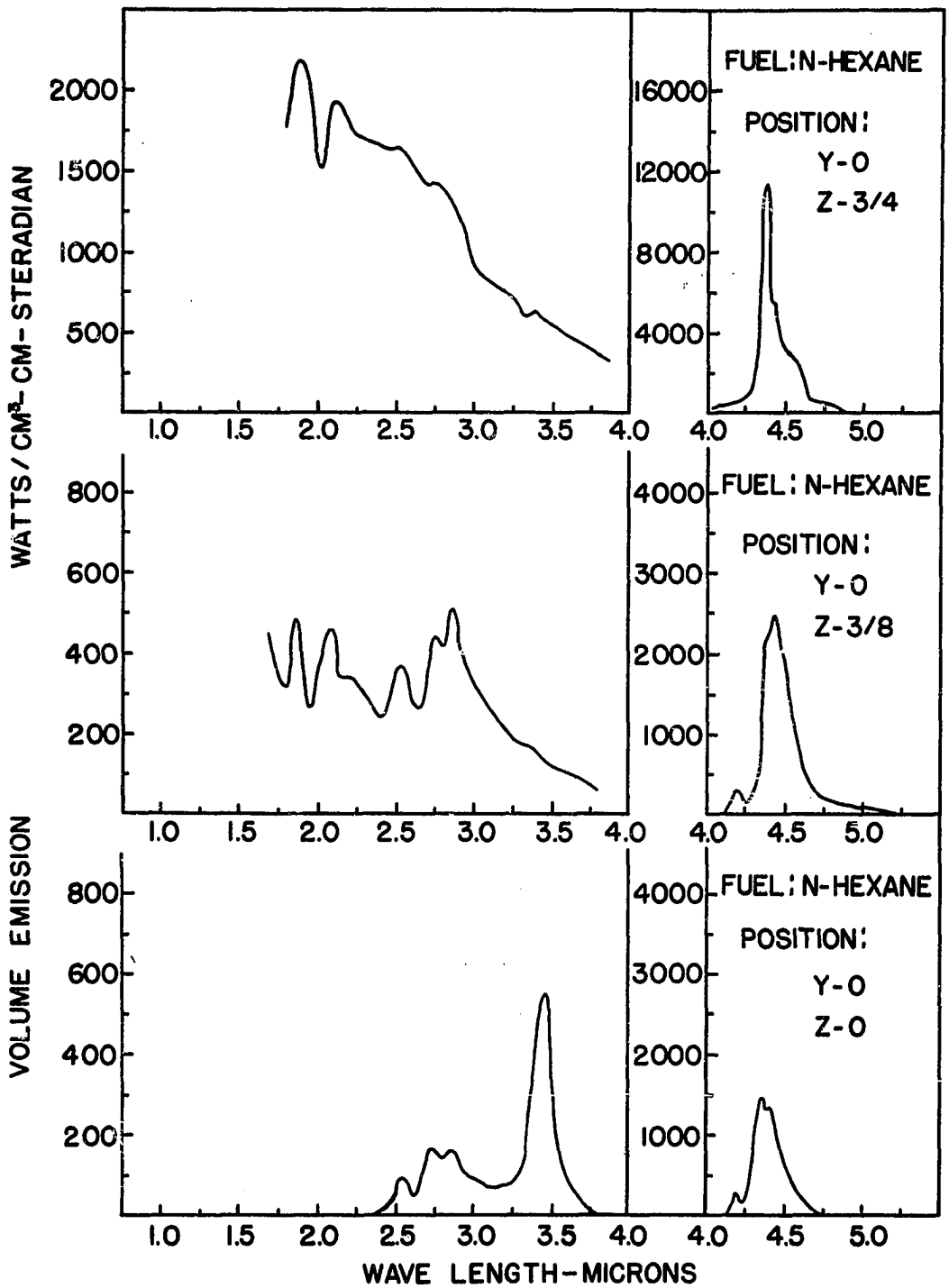


Figure 32. n-Hexane Flame Volume Absorption Coefficient (Y = 0)

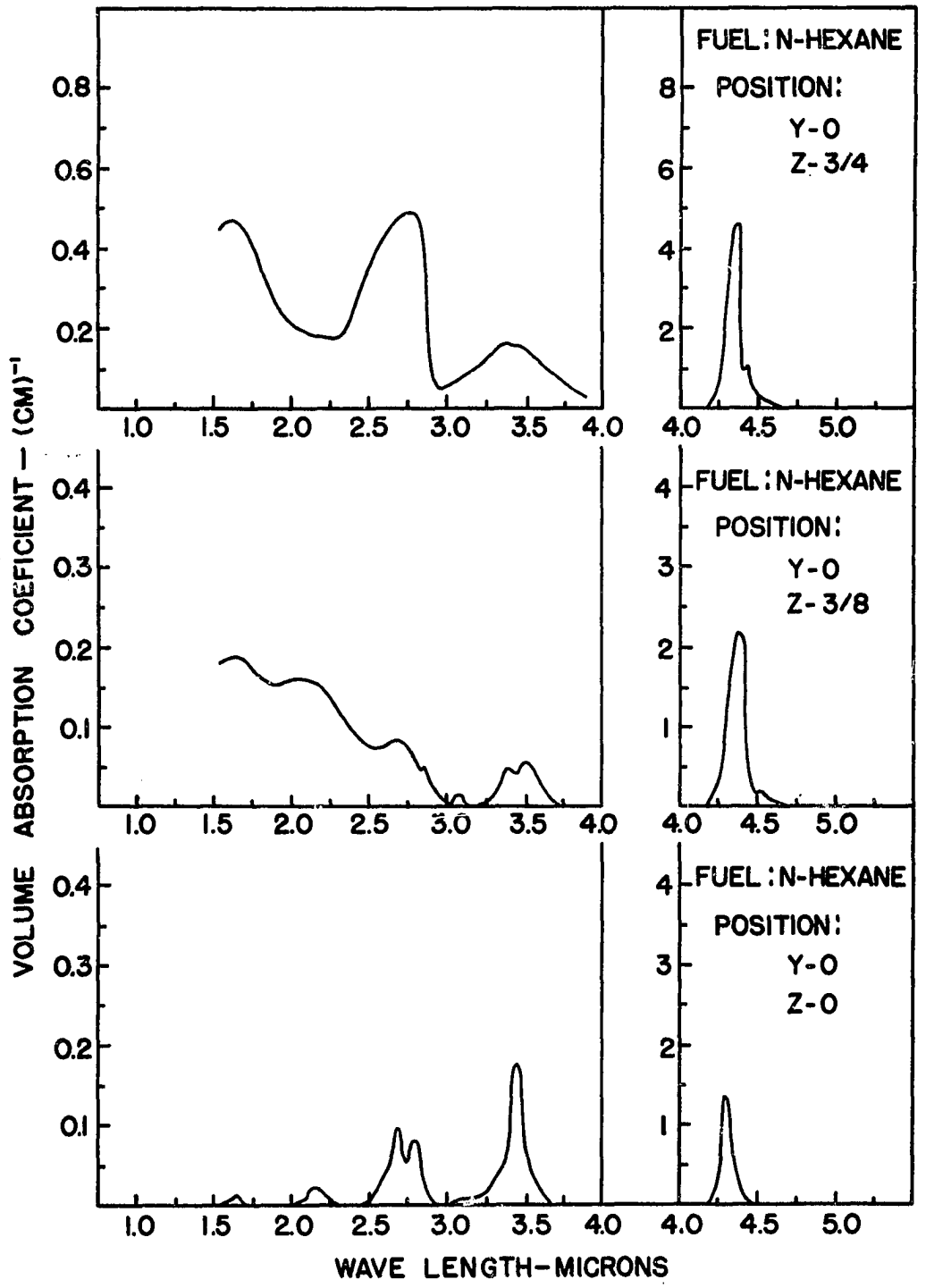


Figure 33. n-Hexane Flame Volume Absorption (Y = 0) Coefficient

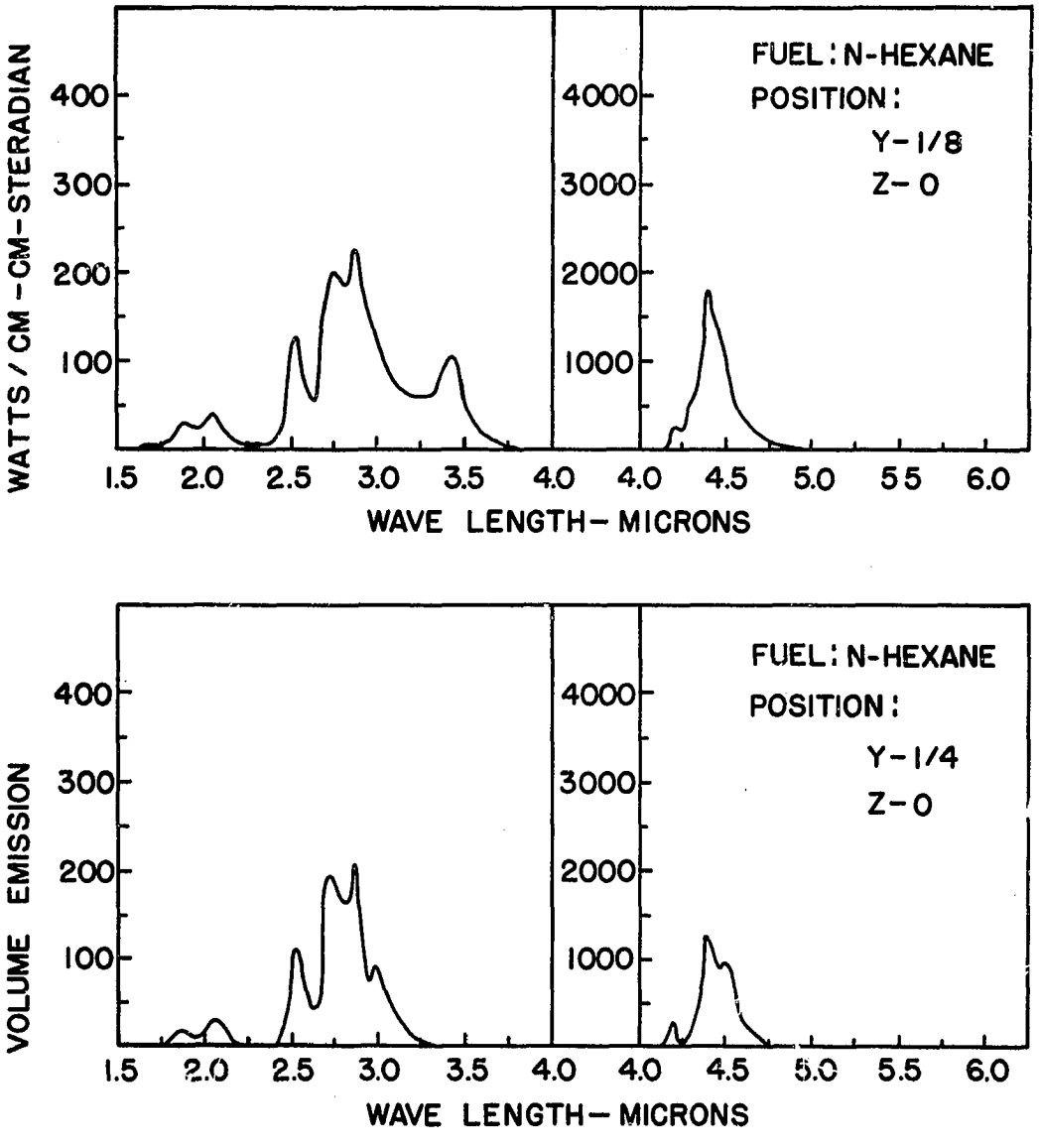


Figure 34. n-Hexane Flame Volume Emission (z = 0)

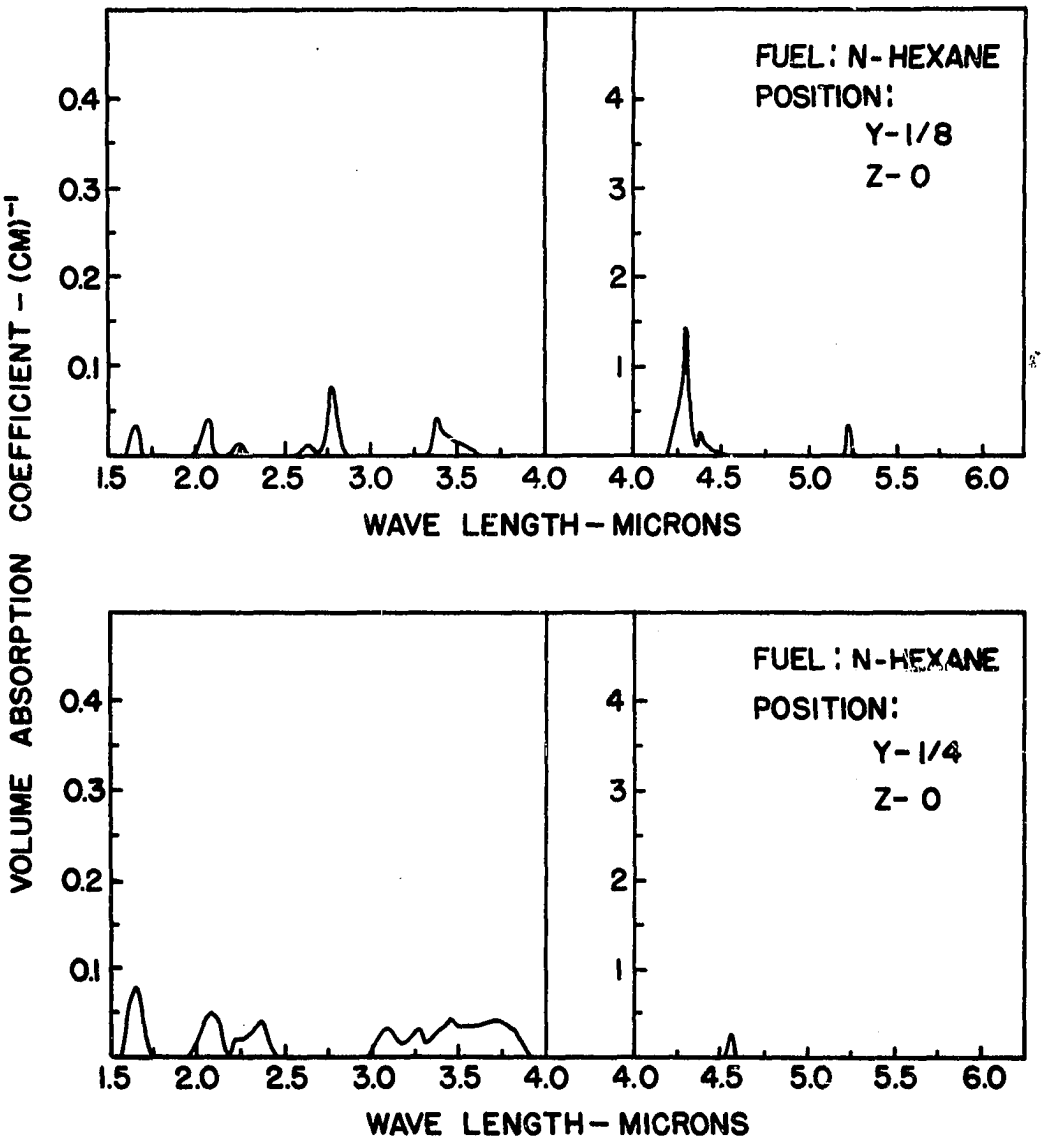


Figure 35. n-Hexane Flame Volume Absorption Coefficient (z = 0)

spectrograms have the general shape of a black body radiation curve except for the presence of the CO_2 peak at 4. 5 microns. The flame height used for cyclohexane and the height used for n-hexane was produced by a 3/4 inch diameter burner and was 1 and 3/8 inches tall. An electrostatic precipitator was constructed above the flame holder to remove the soot produced by the hexane and the benzene flames. The small benzene flames were too unstable to permit spectrograms to be taken of them, so a benzene flame of 2-1/4 inch in height was used. This flame produced large amounts of soot, so only the one data point shown in Figure 36 was taken. This spectrogram has the general shape of a black body radiation curve except for the presence of the CO_2 peak at 4. 5 microns.

The optical path length through the flame for each position was determined by taking a photograph of the flame with a camera. It was aligned so that the optical center line of the camera was in the same plane as the optical center line of the optics system. A Speed Graphic Graphex Camera with a Polaroid 3000 pack film holder was used. The camera was positioned with the lens 20 inches from the flame so an f number of 11 or less was used to reduce the effect of parallax. The diameter of the flame at any height, z, above the base could be determined from the photograph and from this the optical path length for any y, z coordinate position could be determined.

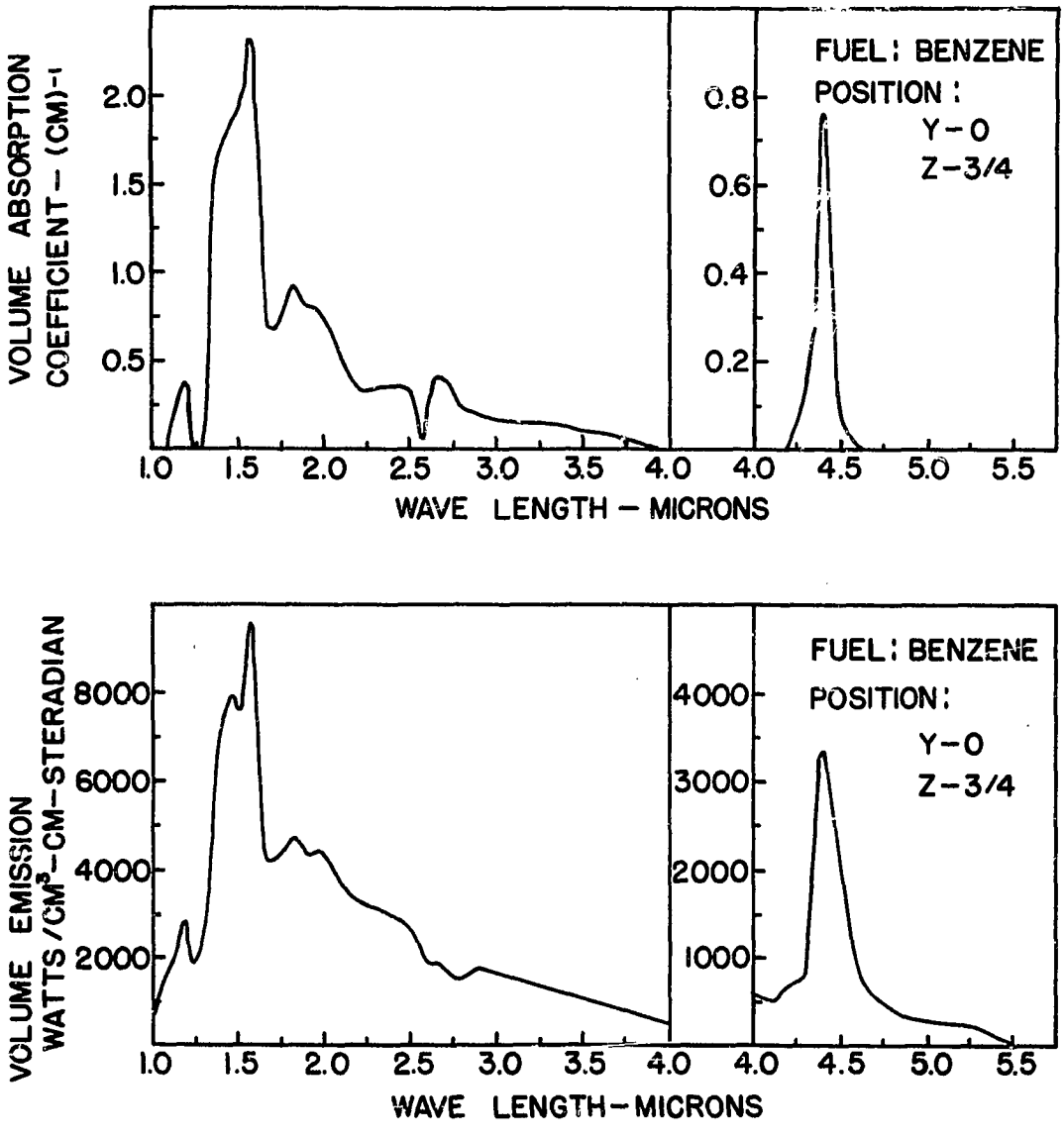


Figure 36. Benzene Flame Volume Emission and Absorption Coefficient

CHAPTER V

DISCUSSION OF RESULTS

The extrapolation program worked out by Shahrokhi (15) to determine the radiative heat flux to a target from an arbitrary size flame was based on the following considerations. The flame was characterized by either a cylinder, a cone, or a sheet of flame for computational purposes. The diffusion flame produced from a cylindrical burner was considered to occupy a cylindrical volume having a mean diameter and a mean height. These mean values were determined by observing several pictures taken of the flame with a short exposure time. Although the flame tilted and changed shape somewhat, it was still found to occupy approximately the same volume. The diameter and height of cylinder superimposed on these several pictures were averaged to determine the mean diameter and height used in computing the heat flux from the flame.

The monochromatic intensity being radiated by the flame is given by equation 7 where x is the optical path length through the portion of the flame being observed. The monochromatic flux to a target was computed by sub-dividing the flame into zones and multiplying the

intensity emitted by that zone times the solid angle from the target subtended by the zone times the cosine of the angle between the normal to the target and the central direction of the solid angle.

For a cylindrical flame, the flame was sub-divided into N vertical strips and M horizontal strips on the plane through the centerline of the cylinder facing the target. Figure 37 shows the geometry used to compute the flux from a cylindrical flame. The total monochromatic flux at the target is given by

$$q_\nu = \sum_{m=1}^{M} \sum_{k=1}^{K} \frac{2J_{\lambda mk}}{\beta_{\lambda mk}} (1 - e^{-\beta_\lambda a_{mk}}) \Omega_{mk} \cos \theta_{mk} \qquad (54)$$

where

β_λ = monochromatic volume extinction coefficient

J_λ = monochromatic volume emission coefficient

a_{mk} = average optical depth of the (m, k) zone

Ω_{mk} = solid angle subtended by the (m, k) zone

θ_{mk} = angle between the normal to the surface and the central direction of the solid angle

For a cylinder of height H and radius R divided into N vertical strips and M horizontal strips the following quantities were defined for a target at a distance D away from the edge of the flame.

$$K = \frac{N}{2}$$

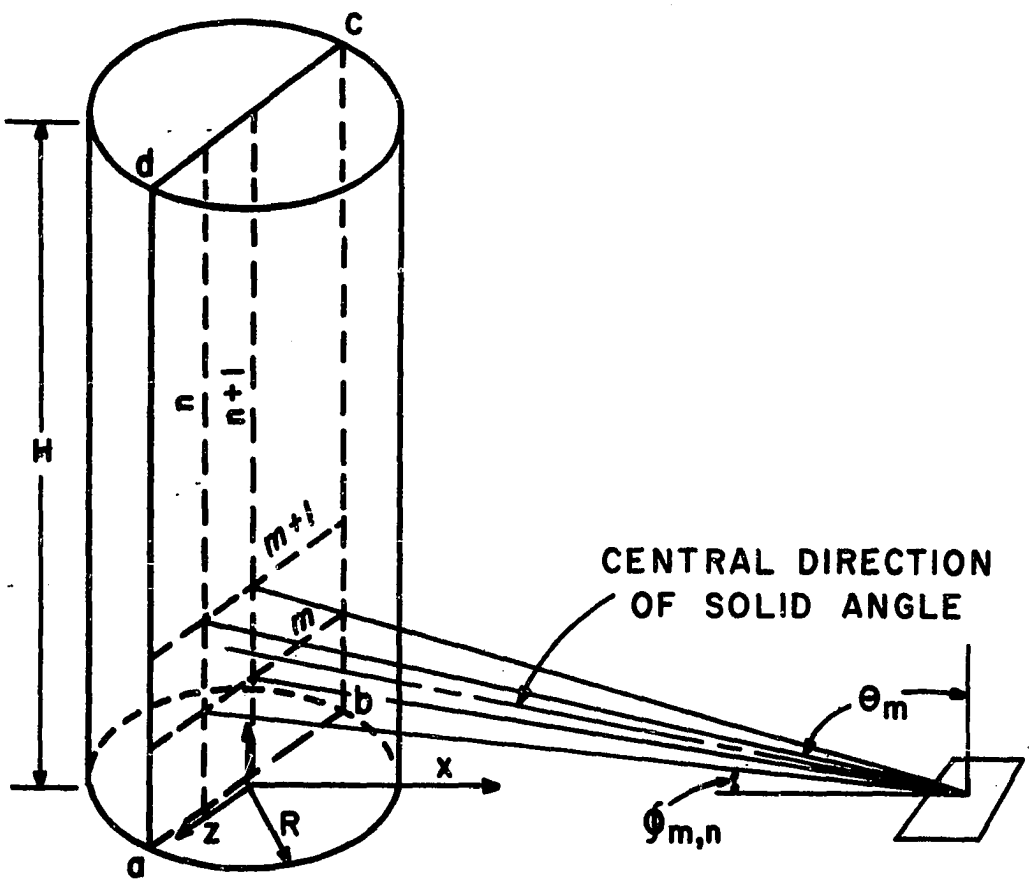


Figure 37. Geometry for Cylindrical Flame

$$H_m = \frac{H}{M} \quad \text{for } m = 1 \text{ to } M$$

$$R_k = \frac{R}{K} \quad \text{for } k = 1 \text{ to } K$$

$$\tan \sigma_{mk} = \frac{R - (k - 1/2)\, R_k}{\left[(D + R)^2 + \left[(m - 1/2) H_m\right]^2\right]^{1/2}}$$

$$\tan \Phi_m = \frac{(m - 1/2)\, H_m}{D + R}$$

$$\sin \beta_{mk} = \frac{D \sin \sigma_{mk}}{R}$$

$$\sin \gamma_{mk} = \frac{(R + D) \sin \sigma_{mk}}{R}$$

In terms of these quantities the solid angle is defined by:

$$\Omega_{mk} = \frac{R_k H_m \sin(\frac{\pi}{2} - \sigma_{mk}) \sin \Phi_m}{(D + R)^2 + \left[(m - 1/2)\, H_m\right]^2 + \left[R - (k - 1/2)\, R_k\right]^2} \qquad (55)$$

and the optical path length through the flame is given by:

$$a_{mk} = \frac{R}{\sin \sigma_{mk} \sin \Phi_m} \left[\sin (\pi - \sigma_{mk} - \gamma_{mk}) - \sin (\pi - \sigma_{mk} - \beta_{mk})\right] \qquad (56)$$

The total flux at the target was computed by numerically integrating the monochromatic flux using a 40 point Gaussian quadrature technique,

$$q = \int_a^b a(\lambda)\, d\lambda$$

$$x = \frac{2\lambda - a - b}{b-a}$$

$$q = \frac{b-a}{2} \int_{-1}^{1} q(x)\,dx$$

or by the quadrature formula

$$q = \frac{b-a}{2} \sum_{i=1}^{n} w_i\, q(x_i)$$

A computer program was developed to compute the geometric terms for a given flame size and target position. The experimental data for J_λ and β_λ from the spectrometer measurements were used in conjunction with the geometric factors to predict the flux. For the extrapolation on the acetone and methanol flames, J_λ and β_λ were considered to be constants. The values of J_λ and β_λ for the position y = 1/8 inch, z = 3/8 inch were used in the extrapolation program. Figures 13-24 show some variation in the values of J_λ and β_λ for different positions on the acetone and methanol flames. The largest variations from the values of J_λ and β_λ for the y = 1/8 inch, z = 3/8 inch position were found near the boundary of the flame. However, the spectrograms taken at position which were not near a boundary were very similar. The spectrograms for the y = 1/8 inch, z = 3/8 inch position were chosen for the extrapolation because they were characteristic of the spectrograms for any position on the flame other than at a boundary. For sooty flames such as cyclohexane and benzene the values for J_λ and β_λ in the outer cone or sooty

part of the flame were quite different from the values determined from the spectra taken near the base of the flame where the radiation is coming principally from the reaction zone and inner cone of the flame. Thus, when the extrapolation is performed for large diameter sooty flames, the extrapolation grid must also contain the information as to whether the grid points are considered in the outer cone or the inner cone. This is why the values for J_λ and β_λ have summing subscripts in equation 54.

For acetone and methanol flames the extrapolation program has been completed and the results compared by Tsai (16) to the flux measurements made with a HY - Cal Constantan foil type Pyrheliometer. This pyrheliometer had a quartz window which did not transmit all the radiation. In order to correct for this a transmittance curve was measured for the window. A second integration was performed on the monochromatic flux multiplied by the transmittance of the window at that frequency. This integral then determines the flux passing through the window incident on the pyrheliometer. This correction must be made for flames since the cut-off frequency for quartz lies in the same spectral region as the CO_2 radiation. Figure 38 shows the total predicted flux from equation 15, the values measured with the pyrheliometer and the total predicted transmitted flux, which is the predicted flux times the transmittance of the quartz window.

Since absolute intensity calibrations were made, the intensity scale for the spectrograms could be determined. Thus, it was possible

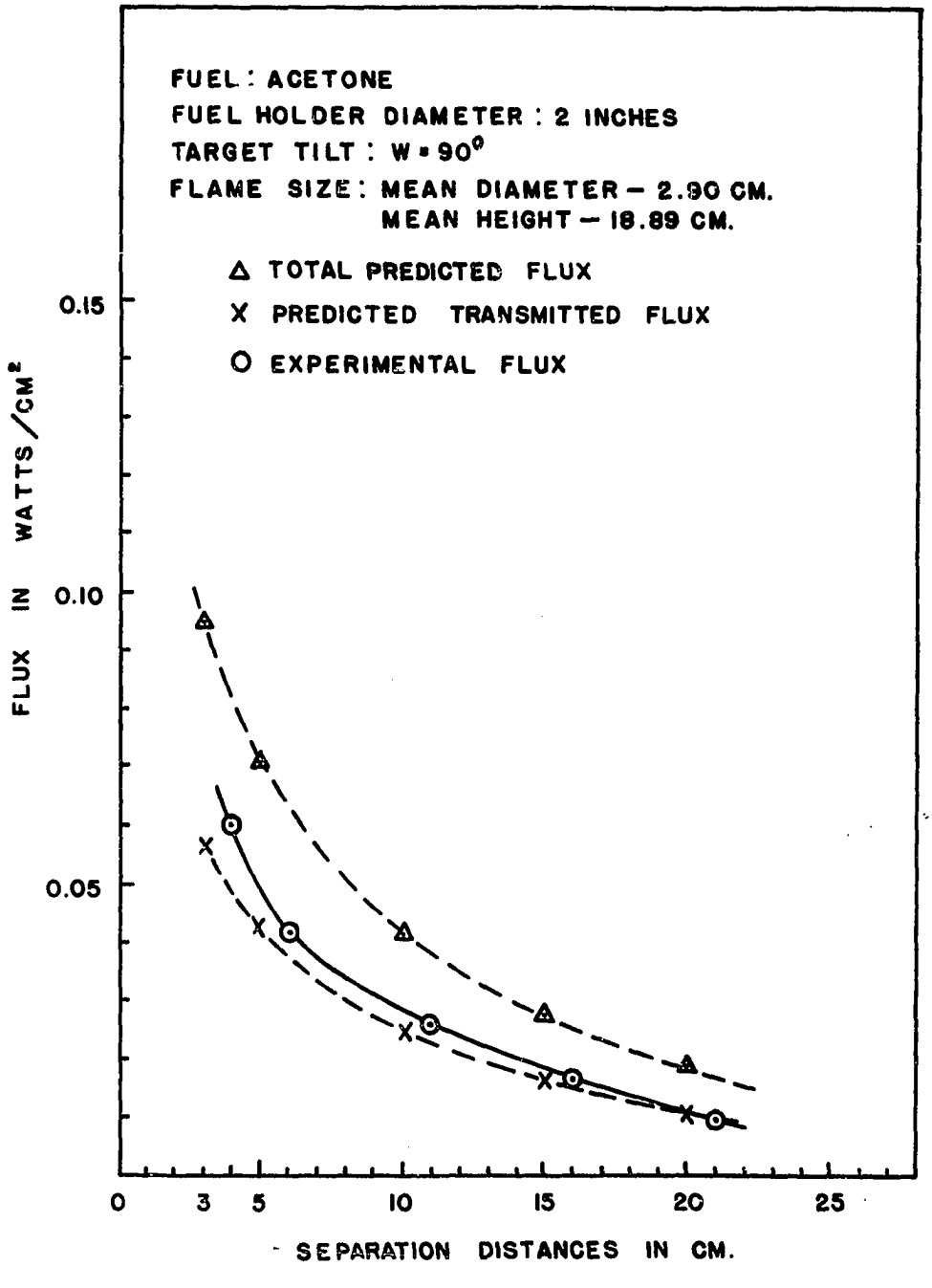


Figure 38. Radiation Flux versus Distance from a Cylindrical Flame

to make some definite arguments concerning the applicability of Kirchhoff's Law to flames. Kirchhoff's Law states that for a system in thermodynamic equilibrium the absorptance and the emittance are equal. Since the monochromatic absorptance and intensity were measured in this experiment and since the monochromatic emittance, ϵ_λ, is defined by:

$$\epsilon_\lambda = I_\lambda / I_{\lambda, bb} \tag{58}$$

the black body intensity, $I_{\lambda, bb}$, could be determined by applying Kirchhoff's Law. Knowing $I_{\lambda, bb}$ the temperature of a black body, T_{bb}, which would emit that intensity could be computed. Figure 39 is a graph of T_{bb} versus wavelength for the y = 0, z = 3/8 inch position for an acetone flame. It was quite obvious that the black body temperature corresponding to the radiation peak at 4.2 to 4.7 microns was much greater than the temperature corresponding to the continuum radiation. The radiation at 4.2 to 4.7 microns was emitted from the vibrational energy levels of the CO_2 molecules. It can be argued that for a system in thermodynamic equilibrium the intensity at any wavelength cannot exceed the black body intensity at that wavelength as computed from the system temperature. For the acetone flame there was no clearly defined system temperature; thus it was concluded that an acetone flame does not represent a system which is in thermodynamic equilibrium.

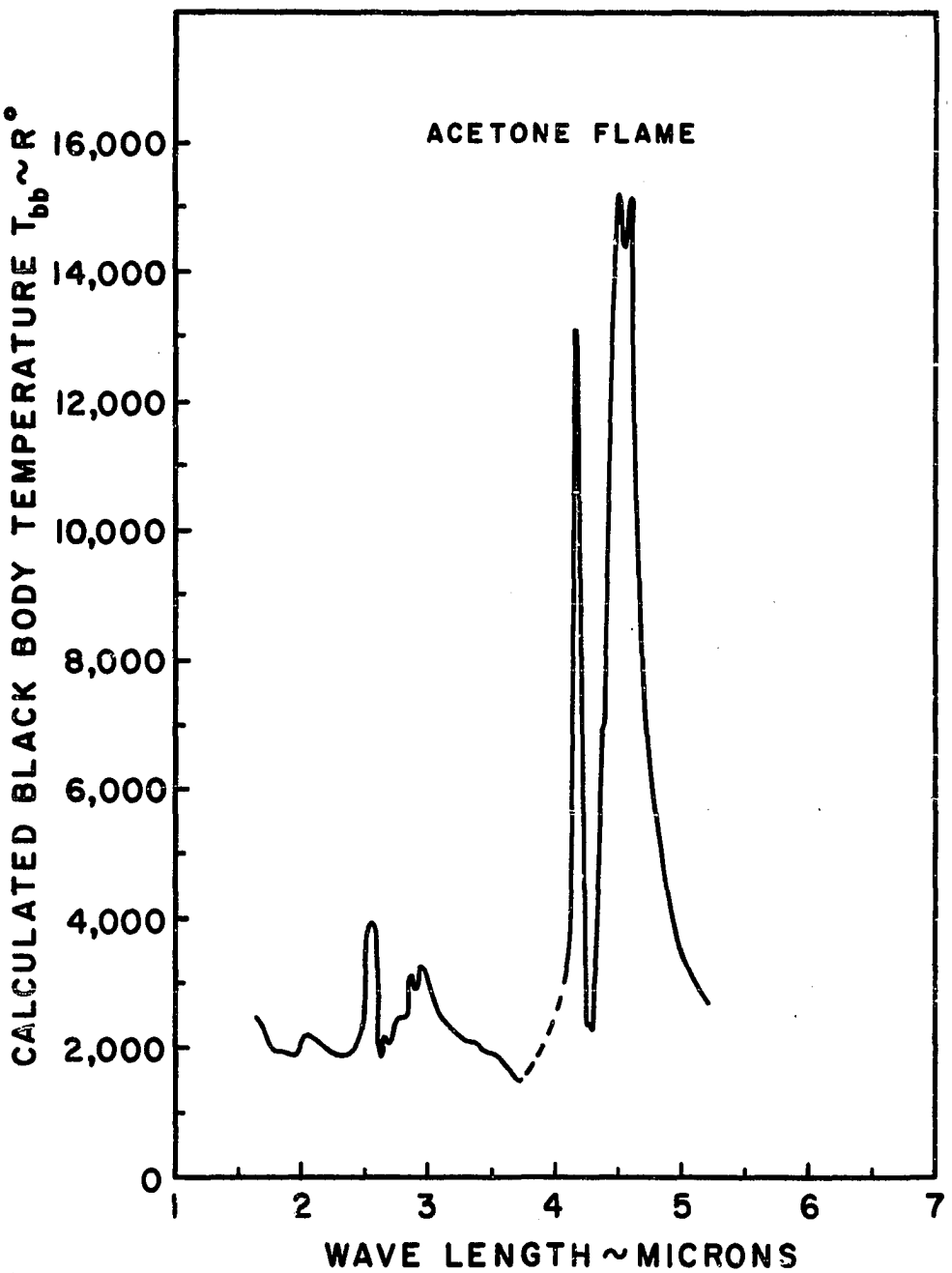


Figure 39. Black Body Temperature for an Acetone Flame

CHAPTER VI

CONCLUSIONS

A method has been presented which accurately predicts the heat flux to targets from flames using transport theory. One advantage of the method is that the average values of J_λ and β_λ may be determined for a given fuel in the laboratory which are useful for extrapolating to larger size flames. The theoretical and experimental flux distribution are shown to be in good agreement by Figures 40, 41.

Another advantage of this method is that only about 100 milliliters of fuel were consumed while making the laboratory measurements. Thus, by using only a small amount of an experimental fuel, its radiative properties may be determined. Also, this method of analysis does not require that the absorbing and emitting medium be in thermodynamic equilibrium, although the method is valid for either the thermodynamic equilibrium or the non-equilibrium case. There are two characteristics of the spectrograms which indicate that the acetone flame is not in thermodynamic equilibrium. Figure 42 has both the volume absorption coefficient and the volume emission plotted as a function of wavelength. It can readily be seen that the peaks of the two curves do not occur at

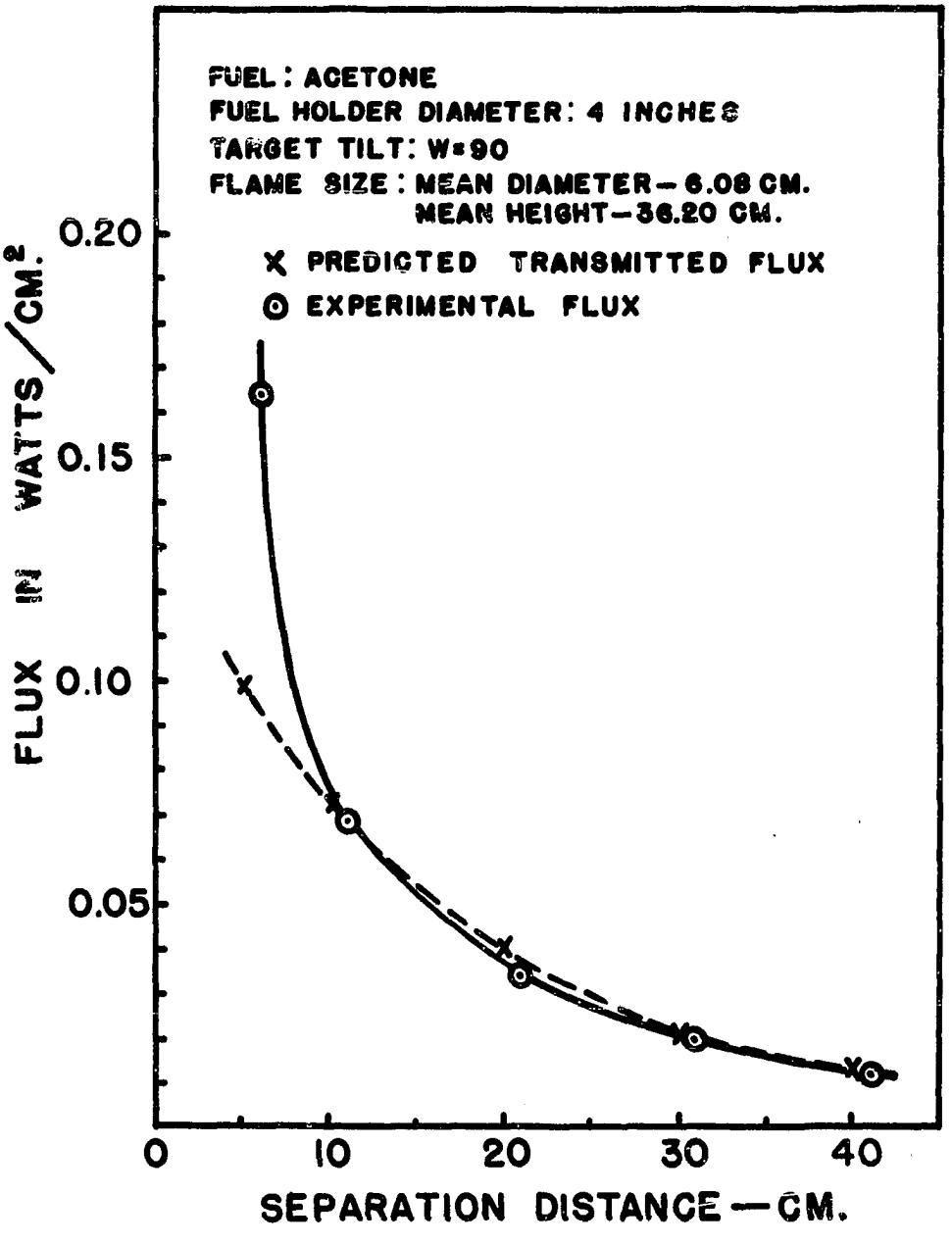


Figure 40. Radiation Flux versus Distance from a Cylindrical Acetone Flame

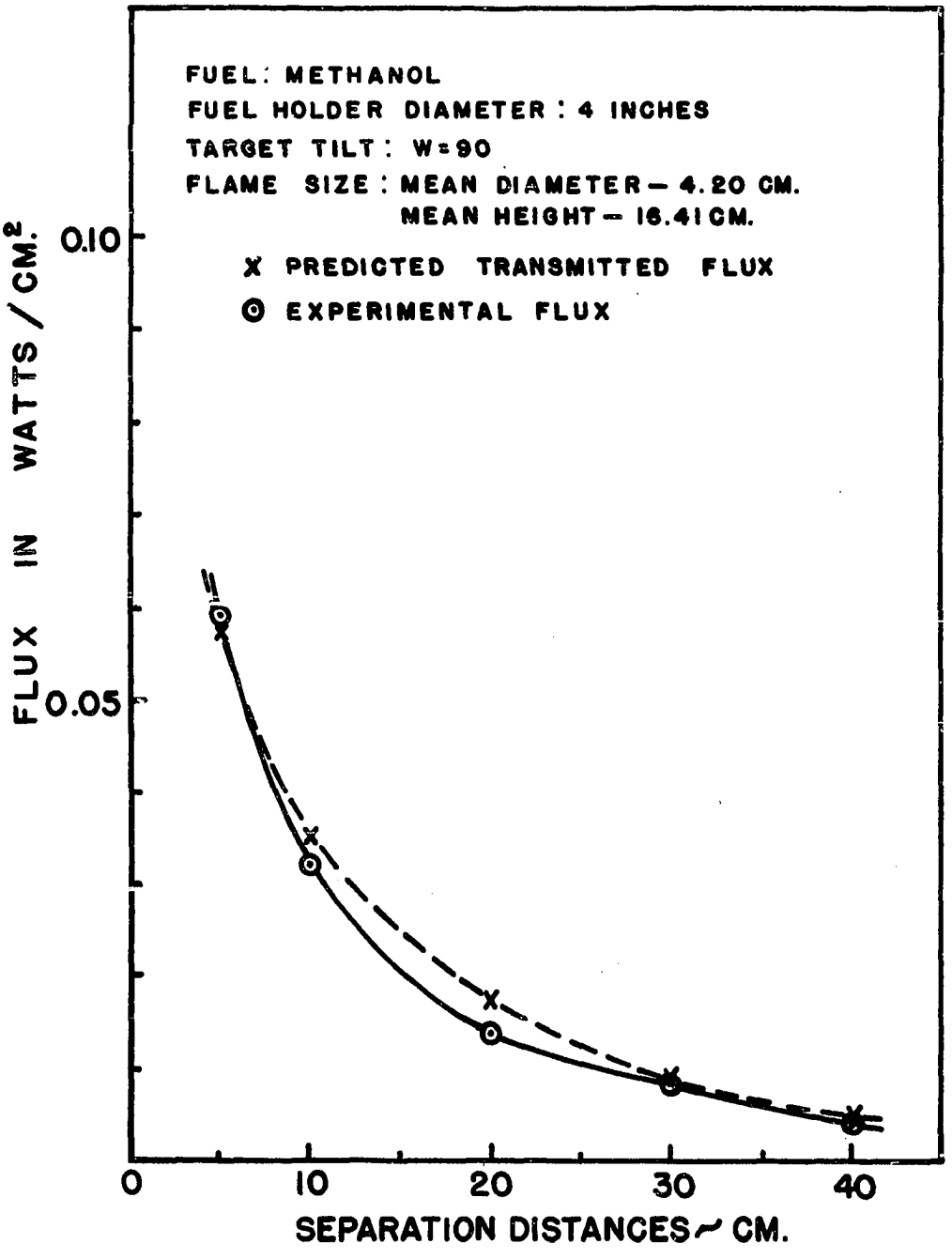


Figure 41. Radiation Flux versus Distance from a Cylindrical Methanol Flame

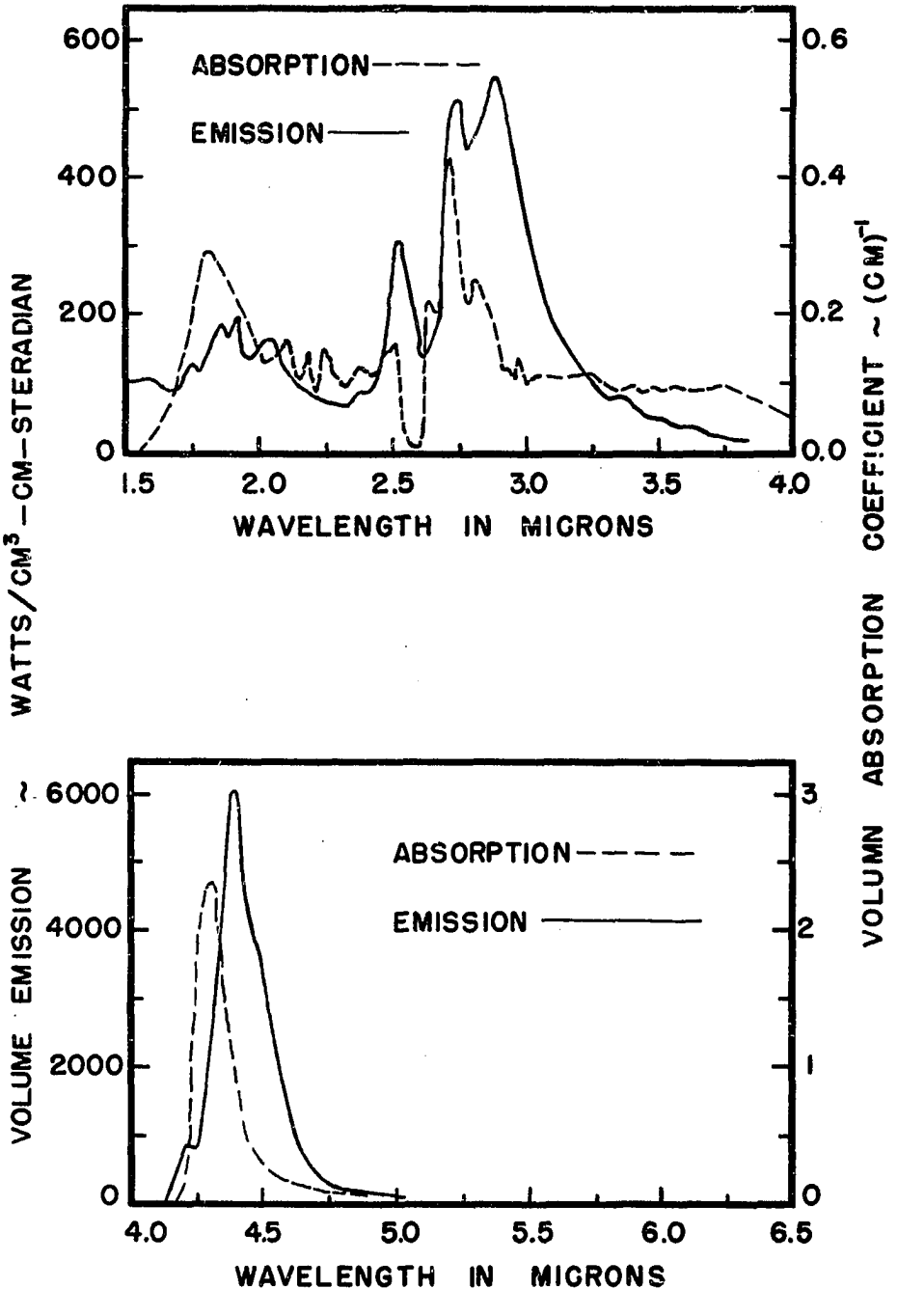


FIGURE 42. COMPARISON OF ABSORPTION AND EMISSION

the same wavelength. Also the large CO_2 vibrational energy emission peak at 4.3 to 4.5 microns indicates that there is a very large population of excited vibrational energy levels. The temperature that would be required for an equilibrium CO_2 gas to emit this amount of energy would be very high. The explanation offered by A. von Engel (17) for the presence of the large amount of CO_2 vibrational energy emission is that due to the relatively long lifetime of the vibrational energy states, it would take a longer time for the CO_2 molecules to equilibrate their energy with the other flame products than the length of time they remain in the flame.

REFERENCES

1. J. Kahrs, "Field Calorimetry/Chemical Studies," Advanced Research Projects Agency, U. S. Army Chemical Research and Development Laboratories, Edgewood Arsenal, Maryland, 1965.

2. L. R. Ryan, G. J. Penzias, and R. H. Tourin, "An Atlas of Infrared Spectra of Hydrocarbon Flames in the 1-5 μ Region," AFCRL-848, Geophysics Research Directorate, Office of Aerospace Research (USAF), Hanscom Field, Bedford, Massachusetts, 1961.

3. H. P. Broida, "Experimental Temperature Measurements in Flames and Hot Gases," Temperature; Its Measurement and Control in Science and Industry, Vol. II, New York: Reinhold Publishing Corp., 1955.

4. E. K. Plyler, L. R. Blaine, and N. Nowak, "Reference Wavelengths for Calibrating Prism Spectrometers," Journal of Research of the National Bureau of Standards, Vol. 58, No. 4, April 1957, pp. 195-200.

5. E. K. Plyler and C. W. Peters, "Wavelengths for Calibration of Prism Spectrometers," Journal of Research of the National Bureau of Standards, Vol. 45, No. 6, Dec. 1950, pp. 462-467.

6. E. K. Plyler, H. C. Allen, Jr., and E. D. Tidwell, "Infrared Spectra of Polycholorobenzeones," Journal of Research of the National Bureau of Standards, Vol. 58, No. 5, May 1957, pp. 255-263.

7. G. R. Harrison, R. C. Lord, and J. R. Loofbourow, Practical Spectroscopy, Prentice Hall, Inc., New York, N. Y., 1948, pp. 118-119.

8. B. Rossi, Optics, Addison-Wesley Publishing Co., Inc., Reading, Mass., 1959, pp. 202-208.

9. E. C. C. Baley, Spectroscopy, Vol. 1, Longmans, Green and Co. Ltd., London, 1927, p. 86.

10. F. A. Jenkins and H. E. White, Fundamentals of Optics, McGraw-Hill Book Co., Inc., New York, 1957.

11. G. S. Monk, Light Principles and Experiments, McGraw-Hill Book Co., Inc., New York, 1937.

12. J. Morgan, Geometric and Physical Optics, McGraw-Hill Book Co., Inc., New York, 1953.

13. Instruction Manual Perkin-Elmer Infrared Equipment, The Perkin-Elmer Corporation, Norwalk, Connecticut, Vol. 3A, pp. 51-52.

14. J. C. Morris, "Comments on the Measurements of Emittance of the Globar Radiation Source," Journal of the Optical Society of America, Vol. 51, July 1961, pp. 798-799.

15. F. Shahrokhi, "Numerical Technique for Calculation of Radiant Energy Flux to Targets from Flames," Ph. D. Dissertation, The University of Oklahoma, 1965.

16. Y. Tsai, "The Prediction of Radiative Heat Transfer from Flames," Master's Thesis, The University of Oklahoma, 1966.

17. A. von Engel and J. R. Cozens, "Flame Plasmas," Advances in Electronics and Electron Physics, Vol. 20, 1964, p. 112.

NOMENCLATURE

a = optical path length through the flame (cm^{-1})

A = area (cm^2)

C_1 = constant in black body radiation law (= 1.177×10^{-12} watts cm^2)

C_2 = constant in black body radiation law (= 2.5776 cm degree Rankine)

E_λ = monochromatic power (watts cm^{-1})

f = focal length (cm)

I_λ = monochromatic intensity (watts cm^{-3} $stearadian^{-1}$)

$I_{\lambda a}$ = monochromatic intensity of flame plus transmitted portion of globar intensity

$I_{\lambda b}$ = monochromatic intensity of flame

$I_{\lambda c}$ = monochromatic intensity of globar

$I_{\lambda r}$ = globar reference monochromatic intensity

J_λ = monochromatic volume emission (watts cm^{-4} $stearadians^{-1}$)

k = thermal conductivity (BTU per hour foot degree Fahrenheit)

n = index of refraction

r = mirror radius (cm)

R = mirror radius of curvature (cm)

s = spectrometer slit width (millimeters)

S = mirror object distance (cm)

S' = mirror image distance (cm)

T_{bb} = black body temperature

T_c = globar temperature

T_r = globar reference temperature

x = optical path length

α = see equation (12)

β = see equation (13)

ϵ_λ = monochromatic emittance

$\frac{d\theta}{dn}$ = dispersion of prism

λ = wavelength (microns)

$\Delta\lambda$ = spectral slit width (microns)

$\Delta\lambda_D$ = dispersion term for spectral slit width (microns)

$\Delta\lambda_R$ = Rayleigh term for spectral slit width (microns)

Ω = solid angle (stearadians)